NOAA Technical Memorandum ERL AOML-35

OCEAN THERMAL AND CURRENT STRUCTURES IN THE TROPICAL SOUTH ATLANTIC RELATIVE TO THE PLACEMENT OF A GRAZING OTEC PLANT

Robert L. Molinari
Frank Chew

Physical Oceanography Laboratory

Atlantic Oceanographic and Meteorological Laboratories
Miami, Florida
January 1979

UNITED STATES DEPARTMENT OF COMMERCE
Juanita M. Kreps, Secretary

NATIONAL OCEANIC AND ATMOSPHERIC ADMINISTRATION
Richard A. Frank, Administrator

Environmental Research Laboratories
Wilmot N. Hess, Director

EXECUTIVE SUMMARY

This report presents the results of the first stage of a multi-stage effort designed to provide ocean thermal and velocity data in the tropical South Atlantic for OTEC. The tropical South Atlantic is one of several areas under consideration for placement of a grazing OTEC plant. In contrast to the moored OTEC plant, a grazing plant can take an active role in acquiring the thermal resource needed to drive the power plant. Because of the ability for self-propulsion, the data requirements for a grazing plant are somewhat different than those for a moored plant. In particular, data are required over a larger spatial area than those in the moored case with knowledge of the details of the horizontal distributions of temperature and velocity as important as data on the vertical distribution. These data requirements are reviewed, with particular reference given both to the importance of advection versus local heating effects in determining the thermal resource in the tropics, and to how the relative importance of these effects impacts upon the OTEC operation.

The meagre data-set available in the area is reviewed to obtain qualitative information on the thermal resource in the region $5^{o}S$ to $10^{o}S$ and $25^{o}W$ to $30^{o}W$. The thermal resource to 900 m ranges from about $23.5^{o}C$ in January through March to a low of $21.5^{o}C$ in July through September. The average standard deviation about the mean resource is about $0.5^{o}C$, with a possible maximum in variability in July-September. The mixed layer depth ranges from an average of 50 m in January-March to an average of 80 m in July-September. The average thermocline depth over all seasons is of the order 115 m.

The current structure also is discussed only in a qualitative manner because of the lack of data. The surface currents appear predominantly zonal to the west, with the possibility of an intermittent eastward flow centered at $5^{o}S$. The current structure in the vertical is complex, with subsurface maxima in the flow to the east at the equator and $5^{o}S$.

Recommendations for further analysis of the historical data set and additional measurements are given. In particular, the data set obtained during GATE should be reviewed. Data collection procedures should include satellite tracked drifting buoys, satellite imagery and current meter moorings. The need for remote sensing is particularly important in this region because of the cost of ship operations in the remote area.

TABLE OF CONTENTS

	Page
Executive Summary	iii
Table of Contents	v
List of Figures	vi
List of Tables	viii
I. Introduction	1
II. Physical Oceanographic Data Requirements for a Grazing OTEC Plant	3
III. Background Information	7
Atmospheric Conditions	7
Thermal Conditions	11
Current Conditions	20
Theoretical Studies	25
IV. Climatological Data Representations	27
V. Synoptic Data Representations	40
VI. Summary	40
VII. Recommendations	48
References	55
Appendix 1: Bulk formulas of air-sea interaction	A-1
Appendix 2: GATE and FGGE information pertinent to OTEC data needs.	A-2

List of Figures

		Page
Figure 1:	Potential regions for placement of a grazing OTEC plant, from Avery (1978).	2
Figure 2:	Annual progression of the ITCZ determined visually from the charts of Hastenrath and Lamb(1977).	8
Figure 3:	The curl of the wind stress along 28°W, from Hastenrath and Lamb (1977).	10
Figure 4:	Sea surface temperature minus air temperature (in °C), from Hastenrath and Lamb (1977).	12
Figure 5:	Specific humidity in g/kg, from Hastenrath and Lamb (1977).	13
Figure 6:	Total cloudiness, in tenths from Hastenrath and Lamb (1977).	14
Figure 7:	Mean monthly SST charts (°C) from Neumann (1975).	15
Figure 8:	Same as Figure 7, except for April through June.	16
Figure 9:	Same as Figure 7, except for July through September.	17
Figure 10:	Same as Figure 7, except for October through December.	18
Figure 11:	A schematic representation of the currents in the tropical Atlantic, adapted from Defant (1961).	21
Figure 12:	Surface currents in knots deduced from ship drift reports, from Alencastro (1974).	22
Figure 13:	Directly measured currents observed during GATE, from Bubnov et al. (1977).	23
Figure 14:	The relation of sea surface winds to the North and South Equatorial Countercurrents, from Neumann and Pierson (1966).	26
Figure 15:	Subregions used to generate horizontal distribution maps.	28
Figure 16:	Average temperature profiles for the subregions between 25°W and 30°W (Figure 15), by season.	29
Figure 17:	Mean seasonal distributions of sea surface temperature (°C).	34
Figure 18:	Mean seasonal distributions of temperature (°C) at 900m.	35
Figure 19:	Mean seasonal distributions of temperature (°C) at 1000m.	36

Page

Figure 20: Mean distributions of temperature differences between the sea surface and 900m (^{o}C). 37

Figure 21: Mean seasonal distributions of mixed layer depth (m). 38

Figure 22: Mean seasonal distributions of thermocline depth (m). 39

Figure 23: Sea surface temperatures (^{o}C) observed during Equalant (Kolesnikov, 1973) and September- October, 1971 (Alencastro, 1972). 41

Figure 24: Vertical temperature sections (^{o}C) observed during Equalant I, February-March, 1963, and sea surface temperature traces (Kolesnikov, 1973). 43

Figure 25: Same as Figure 24, except for Equalant II, August 1963. 44

Figure 26: Zonal temperature sections (^{o}C) from March, 1957 (Fuglister, 1960) and September-October, 1971 (Alencastro, 1972). 45

Figure 27: Proposed tracklines for July-August 1978 survey. 51

Figure 28: Proposed tracklines for the 1979 survey. 52

List of Tables

		Page
Table 1:	Thermal data for design	4
Table 2:	Current data for design	5
Table 3:	Approximate mean monthly surface winds in the region $20^{o}W$ to $30^{o}W$.	9
Table 4:	Average SST (^{o}C) for the region $25^{o}W$-$30^{o}W$, 0^{o}-$10^{o}S$.	19
Table 5:	Number of data points, N, and standard deviations S. D., for those quadrangles between $25^{o}W$ and $30^{o}W$ with more than five data values.	32
Table 6:	Summary of thermal properties at ATL-1 by subregion (Figure 15).	47
Table 7:	Characteristics of currents in the ATL-1 area and their possible impact on the OTEC operation.	49

I. Introduction

Two modes of operation are being considered for Ocean Thermal Energy Conversion (OTEC) plants. In one configuration, the OTEC plant is moored and the electricity generated by the operation is hardwired to a land based power grid. In the other configuration, the OTEC plant is self-propelled, "grazes", and the electricity generated is used to power an energy intensive manufacturing process, such as the production of ammonia. Previous studies (Avery (1978), for instance) have defined several areas in the tropical oceans which appear suitable as sites for a grazing OTEC plant (Figure 1). This report describes some of the physical oceanographic conditions at one of these sites, ATL-1. ATL-1 is located in the tropical South Atlantic Ocean and extends from approximately $4^{o}S$ to $12^{o}S$, and $25^{o}W$ to $32^{o}W$.

The physical oceanographic data requirements for a grazing OTEC are somewhat different than those for a moored plant. A grazing plant can take an active role in acquiring the thermal resource needed to drive the operation, while a moored plant must accept passively the thermal resource advected to the plant. Therefore, environmental data on a larger spatial scale than in the case of the moored plant are required for input into that portion of the design process which evaluates the effect of the environment on the plant and the effect of the plant on the environment.

The requirement for increased spatial coverage implies increased logistical costs to obtain the required data. The remoteness of ATL-1 from the continental U. S. causes additional operational problems. The travel time from the nearest continental U. S. port is some 10 to 12 days, depending on ship speed, adding significantly to the cost of data collection. More complications arise if current meter or other types of moorings are to be deployed and serviced. Thus considerable care is required to design a cost effective measurement program to obtain the design and impact data necessary to site an OTEC operation at ATL-1.

The report is entitled an interim report because considerable data collected during Gate were not available at the time of this writing. These data, summarized in Appendix I, can add significantly to our knowledge of tropical conditions. They are to be analyzed and included in a final report.

A review of the literature and a portion of the historical data set was conducted as a first step in evolving a suitable measurement program. This report provides the details of the results of this review. An initial observational program is developed based on these results. The program is preliminary in that modifications will occur on the basis of the planned data collection results, and additional results from analysis of historical data, such as the GATE data-set. We begin with some thoughts on data requirements for a grazing plant.

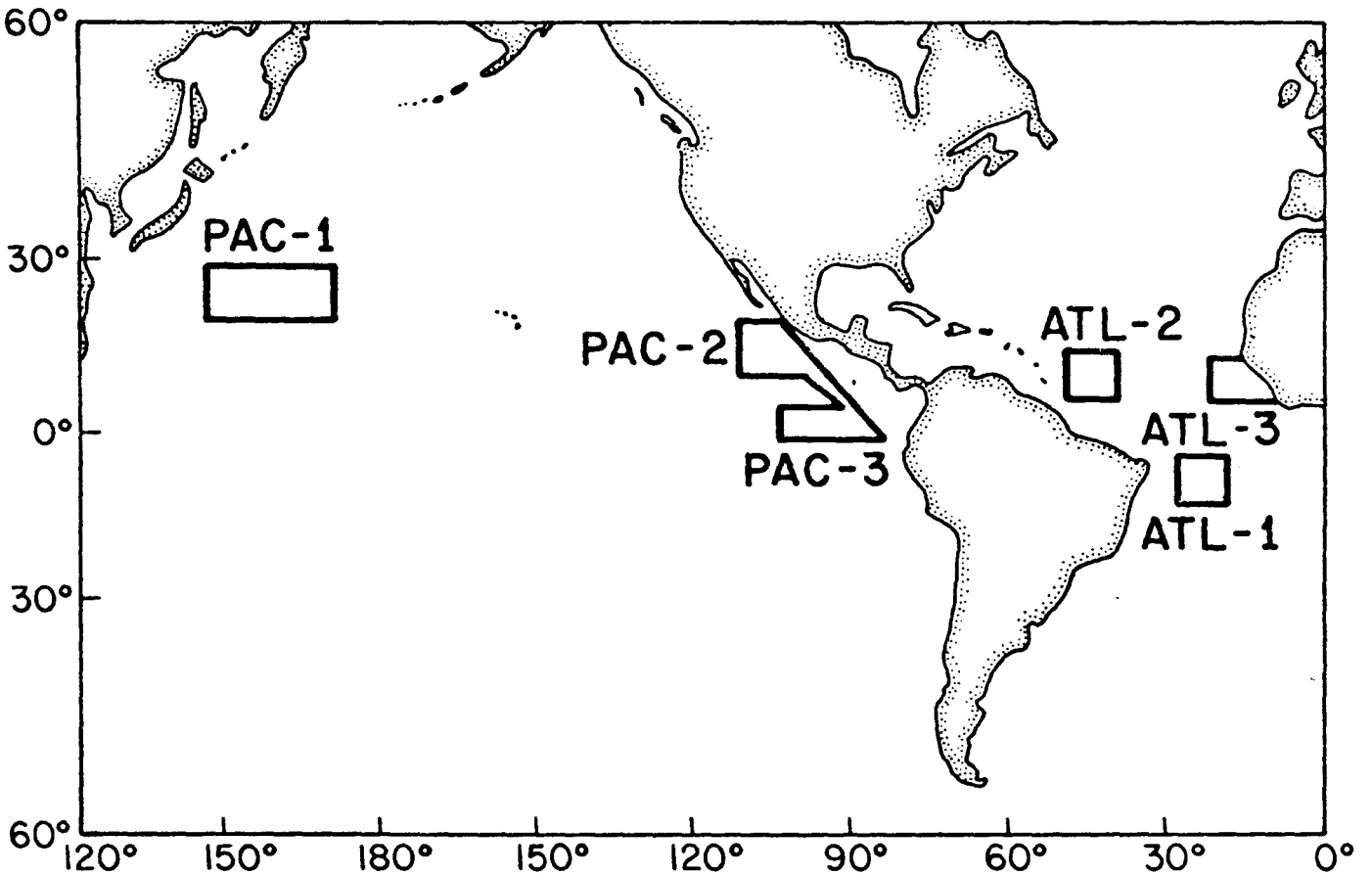

Figure 1: Potential regions for placement of a grazing OTEC plant, from Avery (1978).

II. Physical Oceanographic Data Requirements for a Grazing OTEC Plant

The basic operating principle for the tropical grazing plant is to maximize the thermal resource available to drive the OTEC operation by allowing the plant to take an active role in acquiring the resource. The mobility of the grazing plants dictates the need for data over larger horizontal areas than is required in the moored case, that is, environmental data must be supplied to the designer in three dimensions of space, rather than at a point. The data requirements for a moored plant are given in Tables 1 and 2 (Molinari and Festa, 1978). These variables must be specified throught the grazing area. In addition, the ability to predict these variables becomes a critical requirement as real-time information is required for the daily operation of the plant.

As in the case of the moored plant, the thermal resource is the primary environmental parameter to be defined for use in the design process. Data on the resource are required over the entire ATL-1 region. The data-set should be adequate to define the spatial structure and scales of the thermal resource. For instance, is the large-scale variability in the thermal resource (order of degrees) in the form of patches, tongues, fronts, eddies and/or waves? What is the size distribution of these features, i. e., does large variability occur over small spatial scales (order of kilometers) or only over regional spatial scales (order of hundreds of kilometers)?

Furthermore, data are required on the temporal evolution of the structure of the thermal resource. For example, is the largest signal in the temporal variability seasonal or does significant variability occur on shorter time scales? Data pertaining to these questions and those relating to spatial structure are required to develop efficient grazing strategies. These data are needed in the design effort because the grazing strategies determine, in part, the propulsion requirements.

The grazing plant will draw the warm water resource from a column of fluid of finite thickness, rather than merely a thin surface layer. Therefore, definition of the upper layer thermal structure is required to evaluate the available resource. The thickness and depth of the intake layer is a function of the depth of the warm water intake port. The placement of the port will depend partially on the environmental conditions, so the upper layer should be defined to at least 100m. The mixed layer and thermocline may be located in this layer. The depth of these variables is also required in the design effort (Tables 1 and 2). Data on the temporal and spatial structure of these features is required over the entire ATL-1 region to address the questions given for the thermal resource.

The need to define the subsurface temperature structure precludes the use of satellite imagery to define the thermal resource until the correlation between surface and subsurface structure is determined. As will be discussed, the subsurface thermal structure in the tropics can be more complicated than the surface structure. If similar complications

Table 1: Thermal Data For Design

Thermal Variable	Vertical Spatial Resolution	Horizontal Spatial Resolution	Temporal Resolution	Additional Requirements
1. Temperature Profiles				
a. Operational conditions	NODC standard depths	Site specific	Average daily cycle by month	Variability about daily cycle, long term trends
b. Extreme conditions	NODC standard depths	Site specific	Daily cycle by event	Frequency of occurrence, persistence of event, predictability
2. Mixed layer depth				
a. Operational conditions	±5m	Site specific	Average daily cycle by month	Variability about daily cycle
b. Extreme conditions	±5m	Site specific	Daily cycle by event	Frequency of occurrence, persistence of event, predictability
3. Thermocline depth (seasonal and permanent				
a. Operational conditions	±5m	Site specific	Average daily cycle by month	Variability about daily cycle
b. Extreme conditions	±5m	Site specific	Daily cycle by event	Frequency of occurrence, persistence of event, predictability,
4. Horizontal temperature distribution				
a. Operational conditions	0-500 m@100m intervals	20 km	Monthly	Define structure of frontal systems
b. Extreme conditions	Event dependent	5 km	Event time-scale	Define structure of frontal systems induced by an event

Table 2: Current Data for Design

Current Variable	Vertical Spatial Resolution	Horizontal Spatial Resolution	Temporal Resolution	Additional Requirements
1. Velocity profiles				
a. Operational	0, 30m, 100m, 200m, 300m, 600m, 1000m	Site specific	Tidal (i.e. diurnal)	Additional vertical resolution at sub-surface maxima, countercurrents, etc. Variability about tidal cycle.
b. Extreme	0, 30m, 100m, 200m, 300m	Site specific	Event time-scale	Frequency of occurrence, persistence of event, predictability
2. Distribution of horizontal currents				
a. Operational	Sea surface, discharge depths	25 km	Monthly	Variability about monthly mean
b. Extreme	Event dependent	10 km	Event time-scale	Frequency of occurrence, persistence of event, predictability

occur at ATL-1 they must be quantified in order to use satellite data both in the design of the plant and for operational purposes.

The distribution of currents must be defined in time and space not only in the vertical, as in the case of the moored plant, but also in the horizontal. The distribution in the vertical of horizontal currents is required to compute the current loading on the plant and cold water pipe. The horizontal distribution of currents is needed to compute the probable propulsion requirements for the plant. The structure of the current variability (i.e., waves, fronts, meanders) is also likely to affect the design of the propulsion plant.

Finally, the horizontal distribution of currents is required to determine the trajectories of material discharged from the plant, in order to perform environmental impact studies. These studies are particularly important in view of the fact that although ATL-1 is in international waters, advection can transport plant discharges to the coastal waters of other nations.

The correlation between currents and thermal resource also is required for the design of the grazing plant. If the cold water resource remains relatively constant, the warm water resource determines the available thermal resource. The upper layer temperature structure, including the mixed layer, is a function of the local heat balance, which in turn is composed of a local radiation balance and advection effects. The propulsion requirements will vary depending on the relative importance of advection versus local radiation terms in the heat balance relation. For example, propulsion requirements could be computed if it is known that the dominant changes in thermal resource (order of degrees) occur locally on a seasonal time-scale with the maximum resource migrating over the ATL-1 site in phase with the migration of the thermal equator. Those propulsion requirements would differ from the case in which advection controlled the seasonal resource signal and the plant had to steam against a current to remain in a suitable area.

As will be discussed in a following section, the relative importance of advection versus local effects in tropical oceans is still unknown. This uncertainty will affect the type of instrumentation which can be used to obtain environmental data in the region. For instance, SST data which is not supplemented by additional data or analysis, can not be used to differentiate local from advective features.

The local heat balance also must also be evaluated to determine the environmental impact of OTEC operation. Both oceanographic and meteorologic data are required to compute the terms in the heat balance. An approach to the problem is to use the "bulk formulas" to represent the various types of heat transfer (latent, sensible, etc.), Neumann and Pierson (1966). The bulk formulas require data on air temperature, water temperature, wind speed and relative humidity; in addition, information on short and long wave radiation, and ocean currents are needed. Cost-effective methods to determine these variables over a larg area are required.

III. Background Information

The ATL-1 region is bounded in latitude by $4^{o}S$ and $12^{o}S$, and in longitude by $25^{o}W$ and $32^{o}W$ (F. K. Hill, personal communication). Details of the thermal and current structure of this area are required in the design effort. However, data are needed over a larger horizontal area in order to evaluate the possible impact of OTEC operations on the environment. Therefore, a review of the literature pertaining to the environmental conditions over a larger area than $4^{o}S$ - $12^{o}S$, and $25^{o}W$ - $32^{o}W$ is given.

Atmospheric Conditions

Observational and theoretical studies provide evidence to suggest that the thermal and current structure of the tropical oceans respond more rapidly to atmospheric forcing than do mid-latitude waters (see Philander (1973), for instance). Therefore, a brief review of atmospheric conditions is given.

Figure 2 gives the average monthly progression of the Intertropical Convergence Zone (ITCZ) from Hastenrath and Lamb (1977). North of the ITCZ the winds are from the northeast (NE trades) and south of the ITCZ from the southeast (SE trades). The region of the ITCZ is called the doldrums because of the weak winds (from the east) observed there.

The mean ITCZ is farthest to the north during the summer and farthest to the south during the winter. All references are to the northern seasons. During the winter, the ITCZ crosses the equator at approximately $30^{o}W$. The mean monthly wind speeds and directions observed in the OTEC region are consistent with the climatological position of the ITCZ as seen in Table 3.

The average speed of the SE trades in this region is about 6m/sec. The speeds in the Doldrums are between 2 m/sec and 3 m/sec. The trades are very steady (order of 90%), while the winds in the Doldrums are more variable (order of 50%) (Hastenrath and Lamb, 1977). The results from the GATE program suggest that at least near the equator there is considerable variability in the winds at shorter time periods. Some of this energy appears at frequencies which are similar to prominent frequencies observed in current meter records. For instance, peaks in wind and current energy appear at 4-5 days in various data-sets, (Belewich and Rybnikov 1977).

Temporal and spatial variability in the curl of the wind stress can induce variability in both the thermal and current structure of the upper layers of the ocean (as will be discussed in a following section). The curl of the wind stress over this region is predominantly anticyclonic (Hastenrath and Lamb, 1977). Figure 3 gives a crude represen-

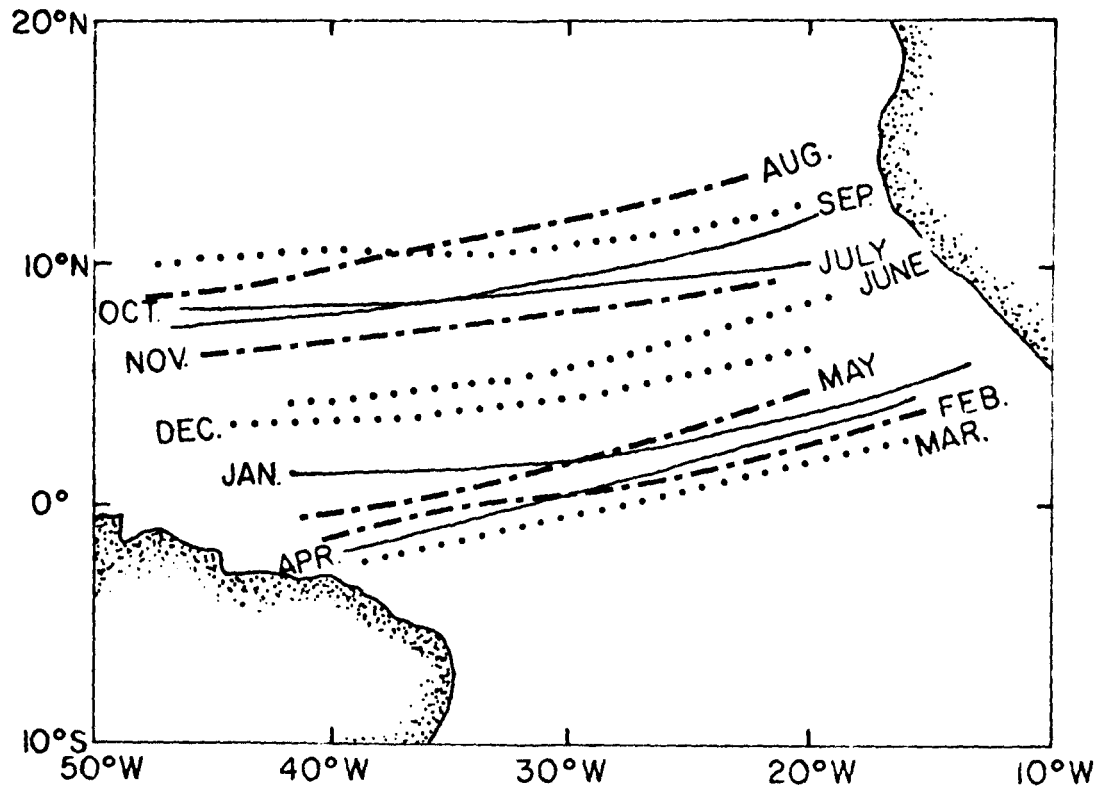

Figure 2: Annual progression of the ITCZ, determined visually from the charts of Hastenrath and Lamb (1977).

Table 3: Approximate Mean Monthly Surface Winds in the Region 20°W to 30°W. Obtained by Visual Inspection of the Charts of Hastenrath and Lamb (1977).

(Speed (m/s)/Direction)

	Latitude Band				
Month	3°N-0°	0°-3°S	3°S-6°S	6°S-9°S	9°S-13°S
January	3/SE	4/SE	5/SE	5/ESE	5/E
February	2/SE	3/SE	5/SE	5/ESE	5/E
March	3/E	3/SE	4/ESE	5/ESE	5/ESE
April	2/E	2/ESE	4/ESE	5/ESE	6/ESE
May	2/E	4/SE	5/SE	6/SE	6/ESE
June	4/SE	5/ESE	6/ESE	6/ESE	7/ESE
July	5/SE	6/ESE	7/ESE	7/ESE	7/ESE
August	5/SSE	6/SE	6/ESE	7/ESE	8/ESE
September	5/SSE	6/SE	6/SE	7/ESE	7/ESE
October	5/SSE	6/SE	6/ESE	7/ESE	7/ESE
November	4/SE	6/SE	6/ESE	6/ESE	6/E
December	4/SE	5/ESE	6/ESE	6/E	6/E

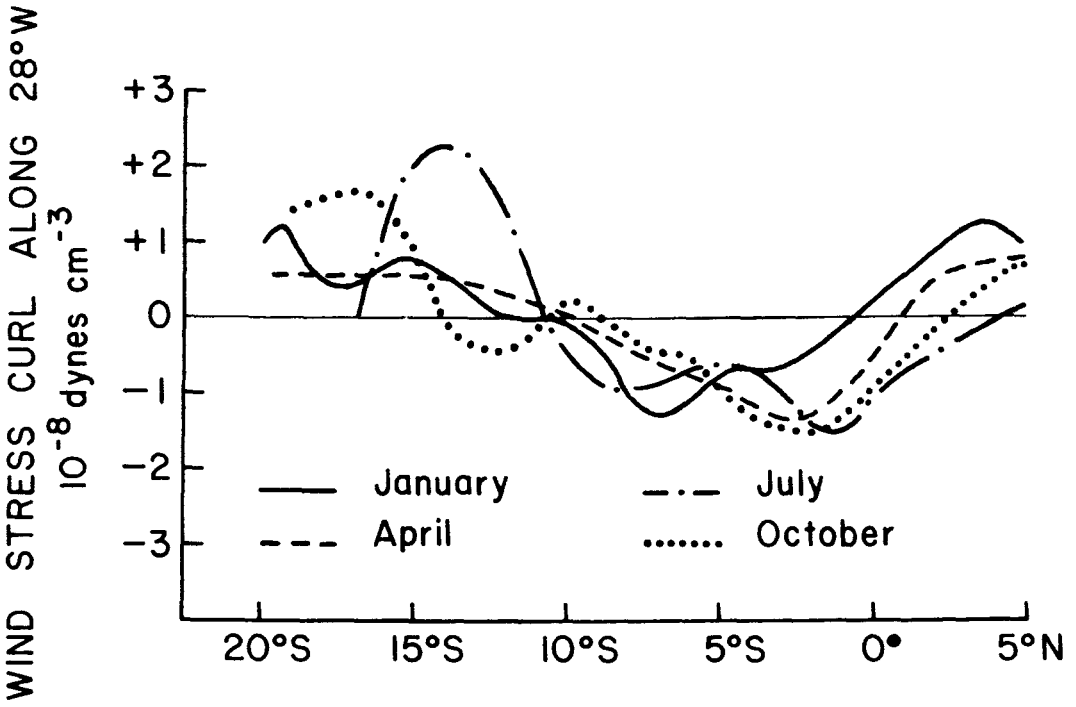

Figure 3: The curl of the wind stress along 28°W, from Hastenrath and Lamb(1977).

tation of the curl as a function of season and latitude, obtained from the charts of Hastenrath and Lamb (1977). There is usually a maximum in the anticyclonic curl in the ATL-1 area. This maximum is closest to the equator during the summer, and farthest south during the winter.

The exchange of energy between ocean and atmosphere which determines the available thermal resource is a function, in part, of several atmospheric parameters. For instance, sea-surface minus air temperature and specific humidity are required to compute the flux of sensible and latent heat (Neumann and Pierson, 1966 and Appendix 1), while total cloudiness is required to compute the local radiation balance. Figure 4, 5, and 6 from Hastenrath and Lamb(1977), show the distribution of average sea-surface minus air temperature, relative humidity and total cloudiness, respectively for four months.

Furthermore, Hastenrath (1977) shows that between 5°S and 10°S and 10°W and 30°W, the air is warmer than the water from September through February. The greatest difference between air and water temperature occurs in June and July, when the water is warmer. As a consequence of the characteristics of the ocean and atmosphere in this region, Hastenrath (1977) finds an annual surplus in the heat budget south of the equator in the Atlantic.

Thermal Conditions

The data coverage in the equatorial South Atlantic is not extensive. However, the available data that have been analyzed indicate complicated ocean thermal and current structures in the vertical direction as well as the horizontal. Figures 7, 8, 9 and 10 give the distribution of mean monthly sea surface temperature (SST) from Neumann (1975). On the average, the lowest temperatures are observed from August through October, and the highest from March through May. This annual cycle is consistent with the seasonal migration of the thermal equator (Neumann, 1975). The cold temperatures appear as a tongue of cooler water along the equator during the summer which extends from Africa to the west. Similarly, south of the cold water tongue centered at 5°S, a tongue of warmer water appears to extend east from the coast of Brazil. The largest spatial gradients in SST occur during the summer months.

The range in the annual cycle of SST is shown in Table 4, which lists the average SST in the region bounded by 25°W and 30°W, and 0° and 10°S. The average values were obtained by inspection of Neumann's (1975) charts. The range in SST is approximately 2.5°C, which is consistent with the 3°C range found in this region by Merle (1977).

Brown (1978) considered the shorter term variability in SST in the region 5°S to 5°N. He found that SST varied on time-scales similar to those observed in the atmosphere (10-15 days) but with much shorter space scales (1800km). These phenomena are intermittent and appear to be advected by surface currents. The magnitude of this variability is

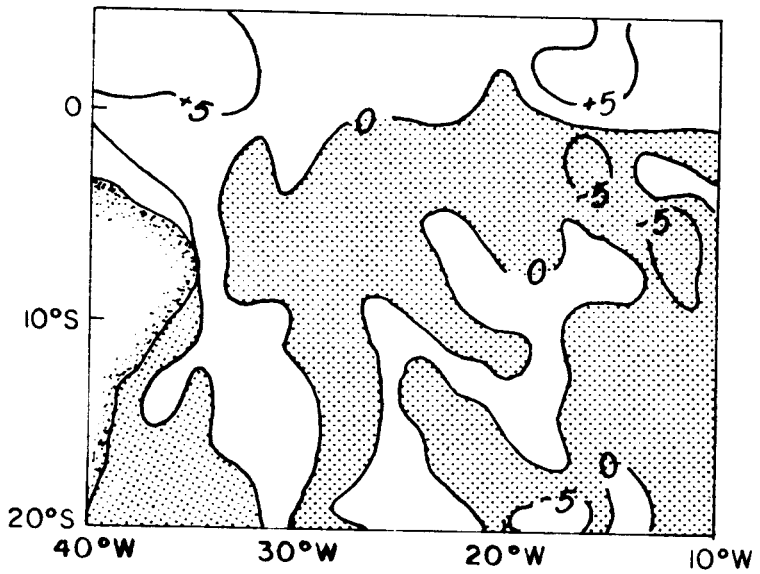

JANUARY

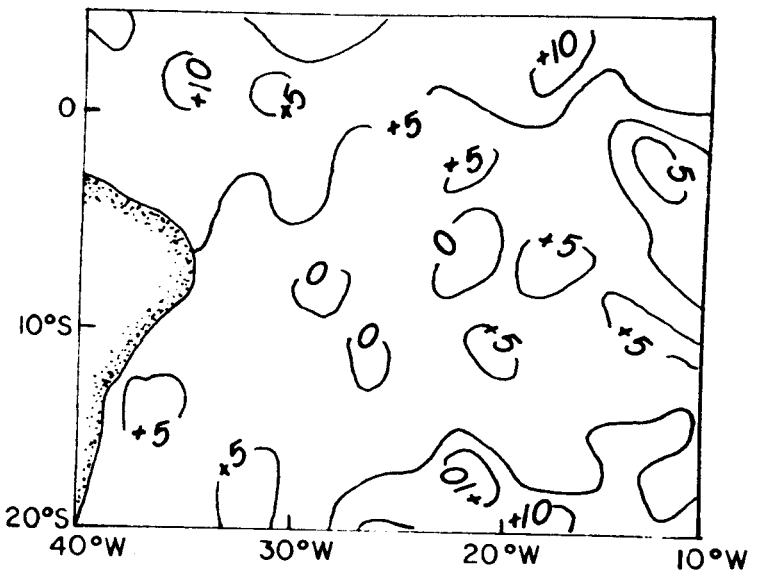

APRIL

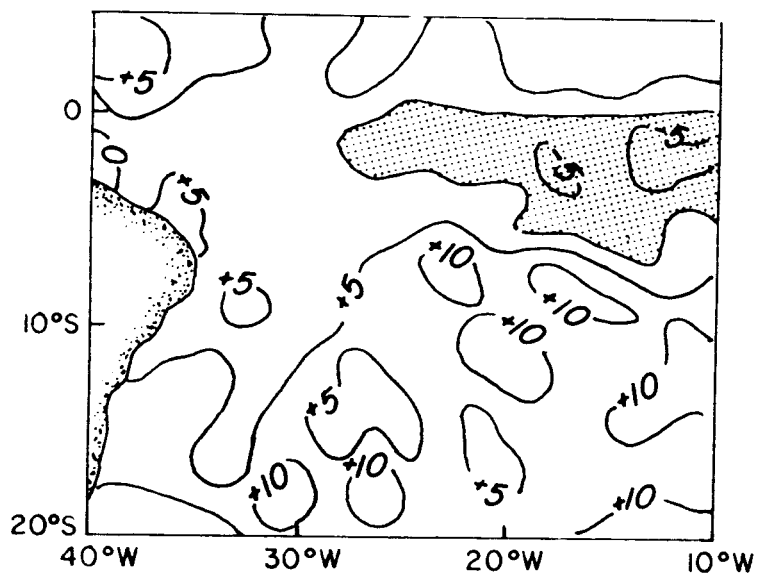

JULY

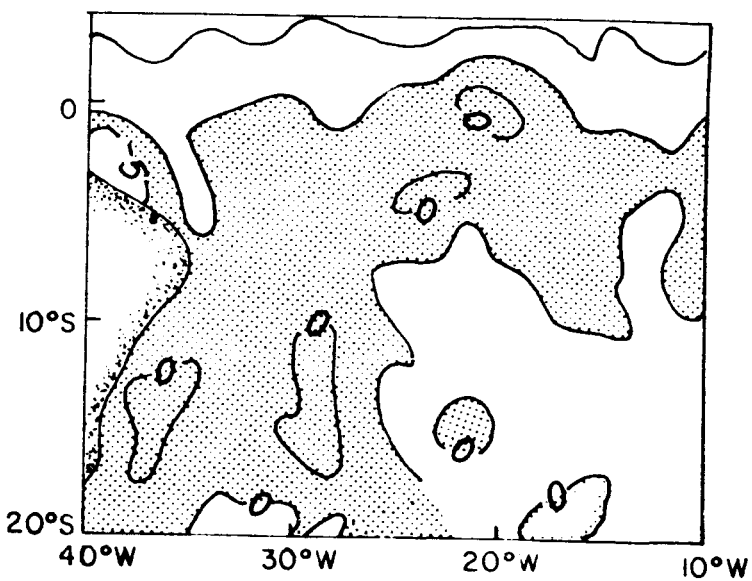

OCTOBER

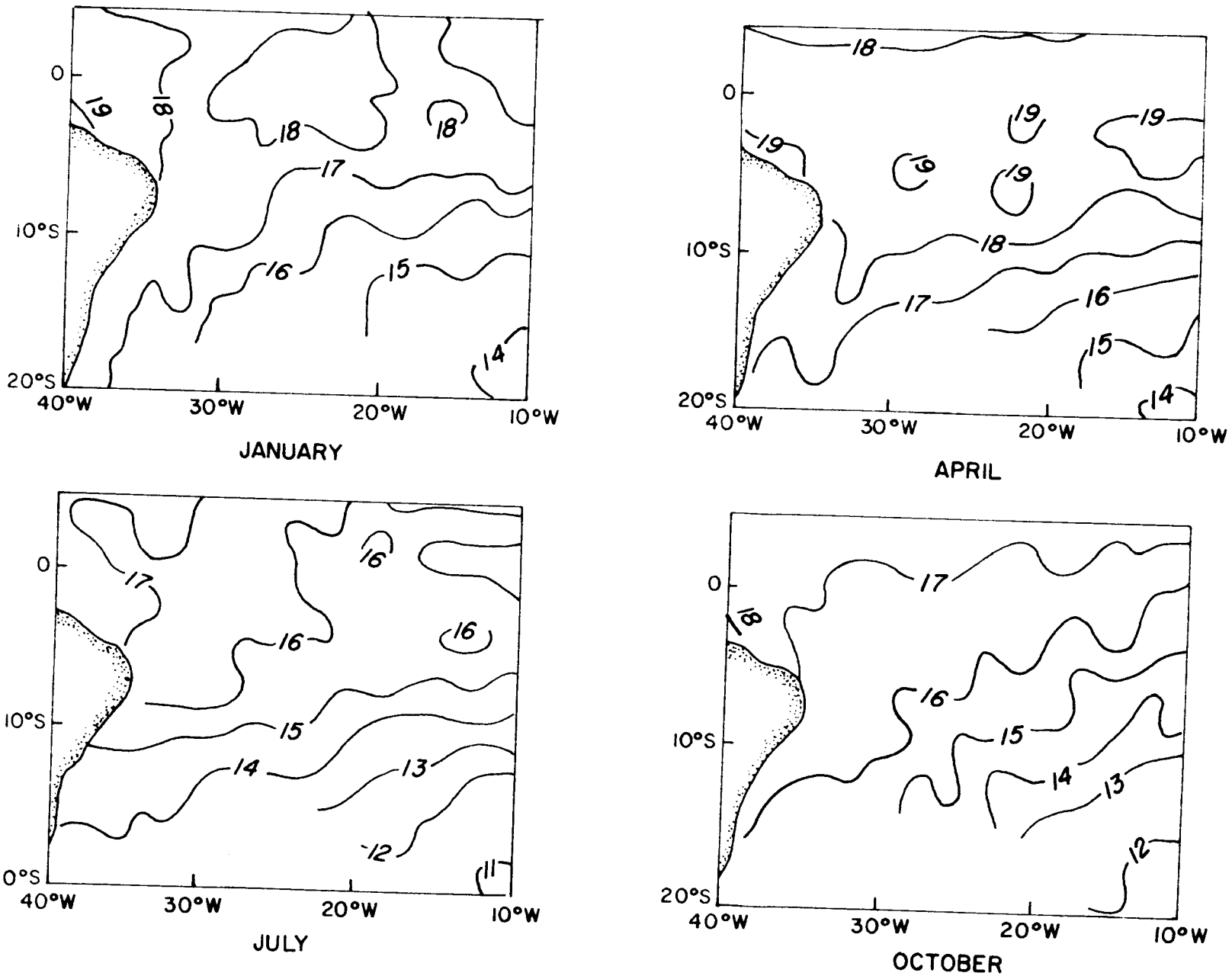

Figure 5: Specific humidity in g/kg, from Hastenrath and Lamb (1977).

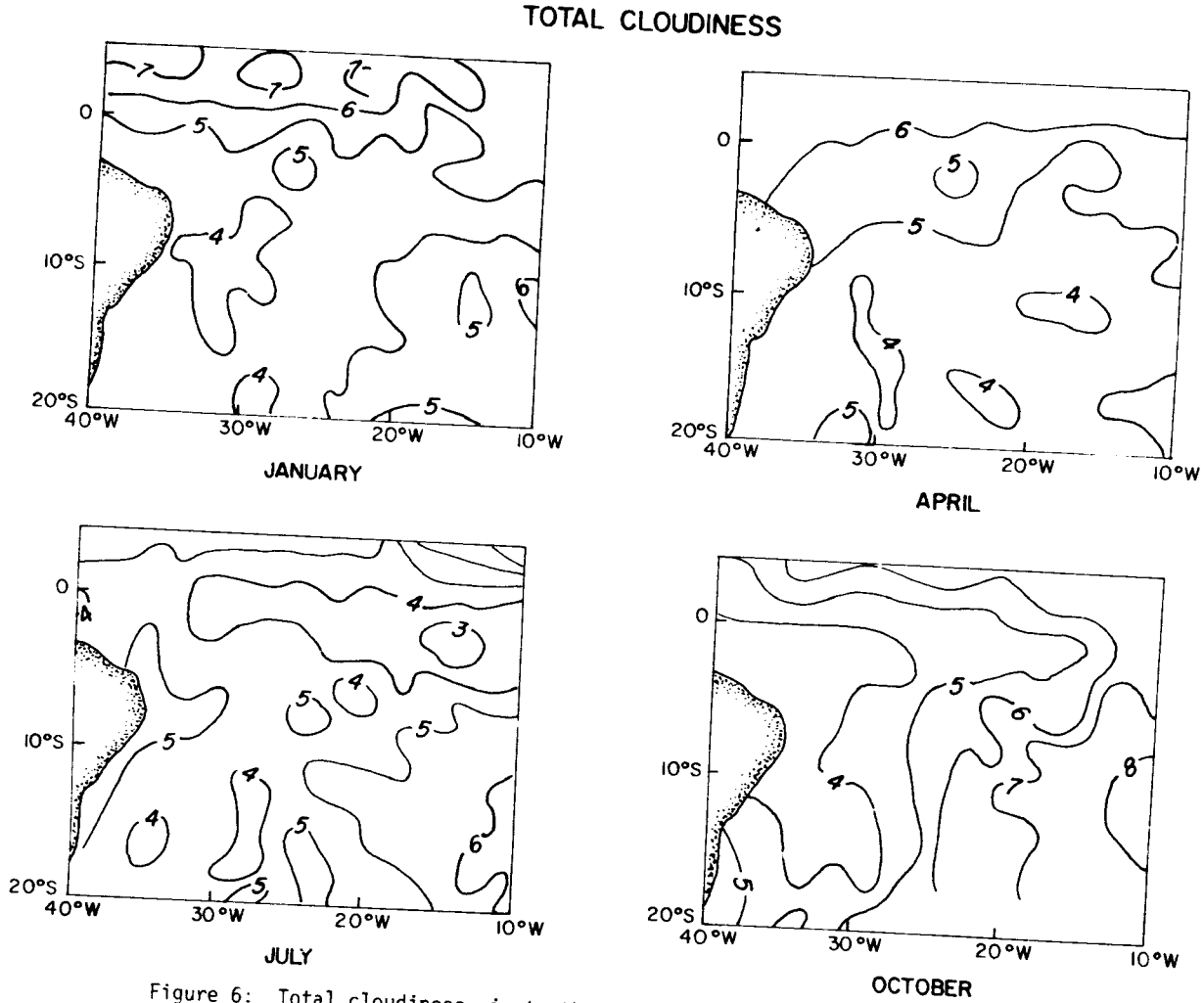

Figure 6: Total cloudiness, in tenths from Hastenrath and Lamb (1977).

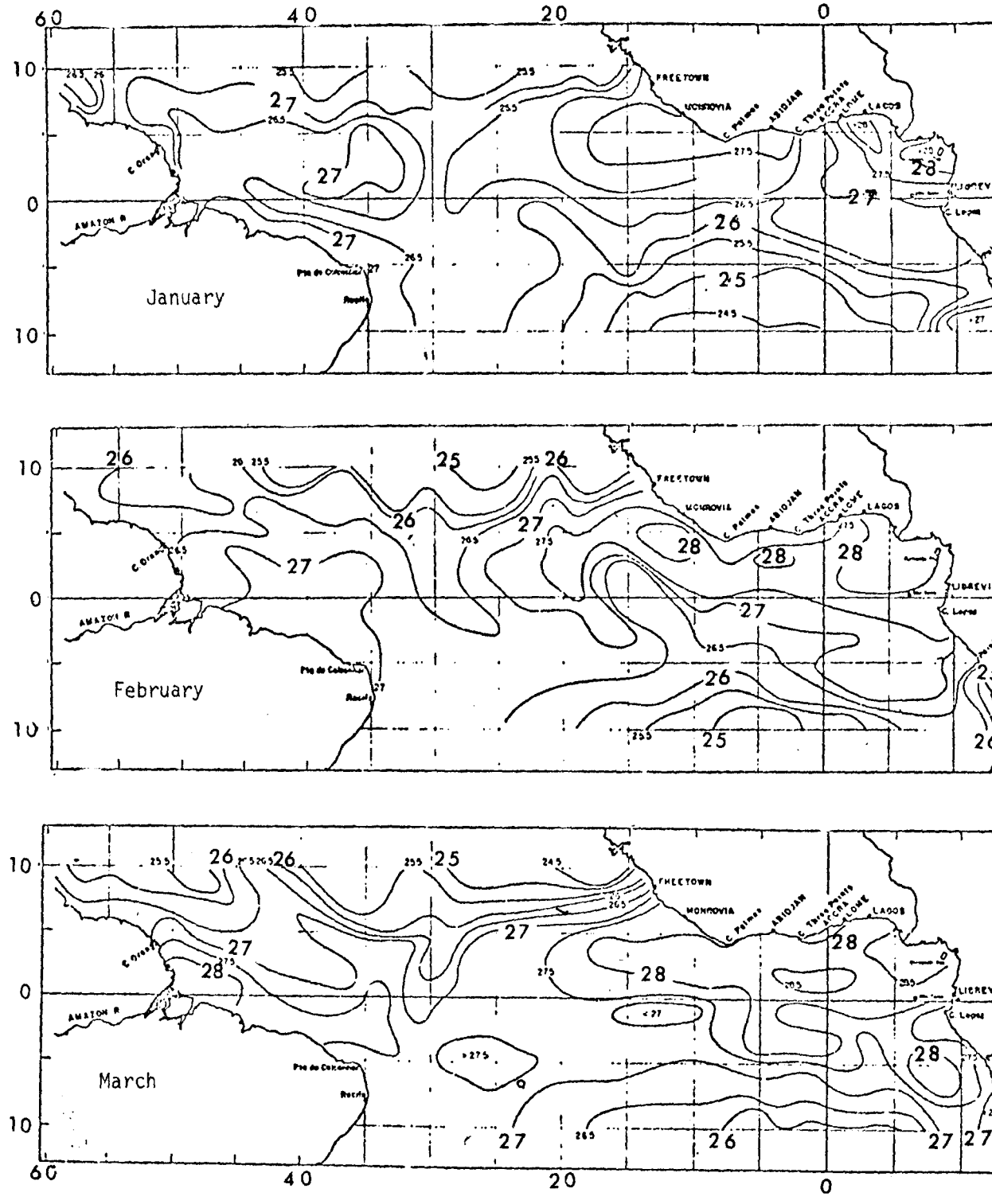

Figure 7: Mean monthly SST charts (^{o}C) from Neumann (1975).

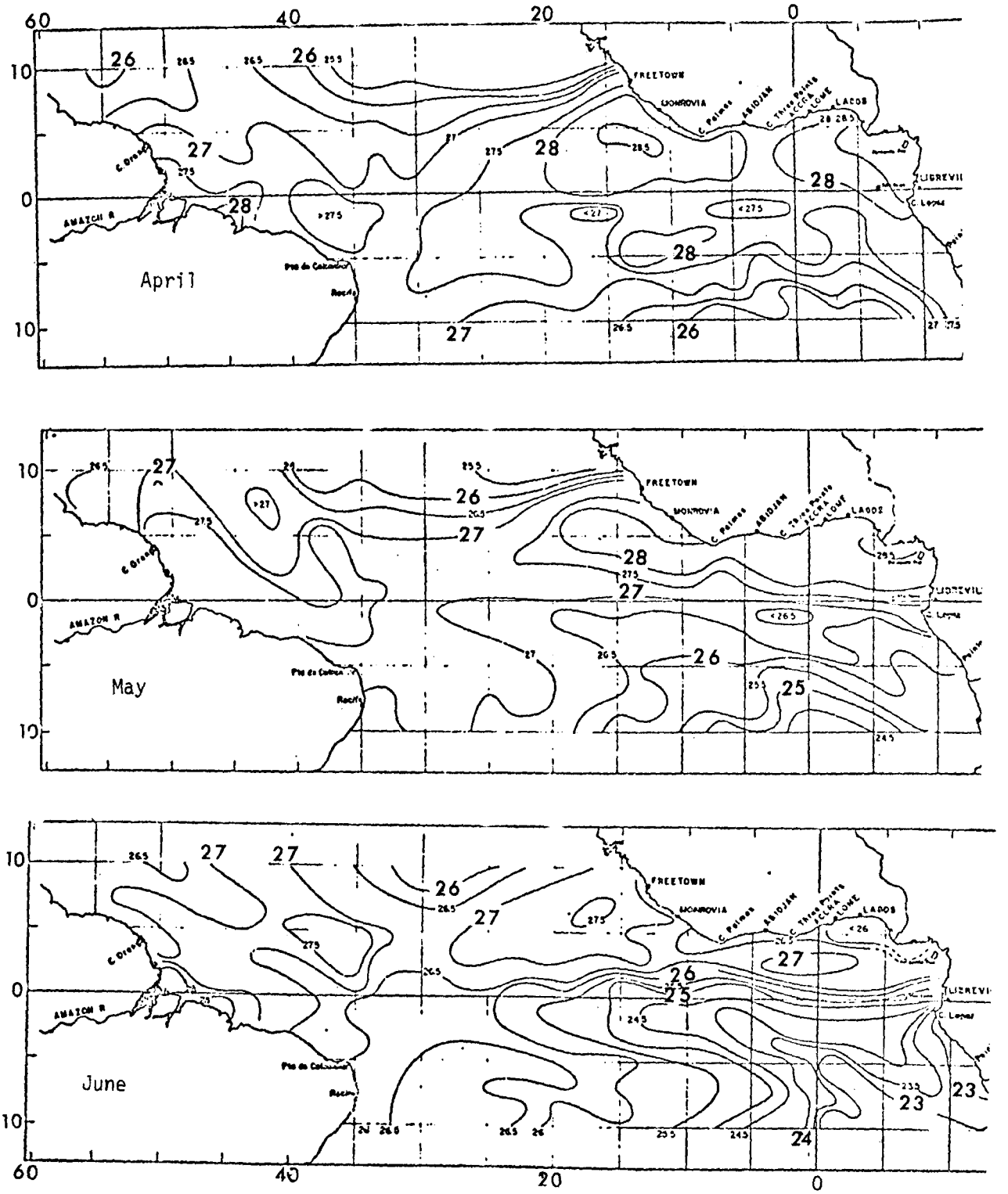

Figure 8: Same as Figure 7, except for April through June.

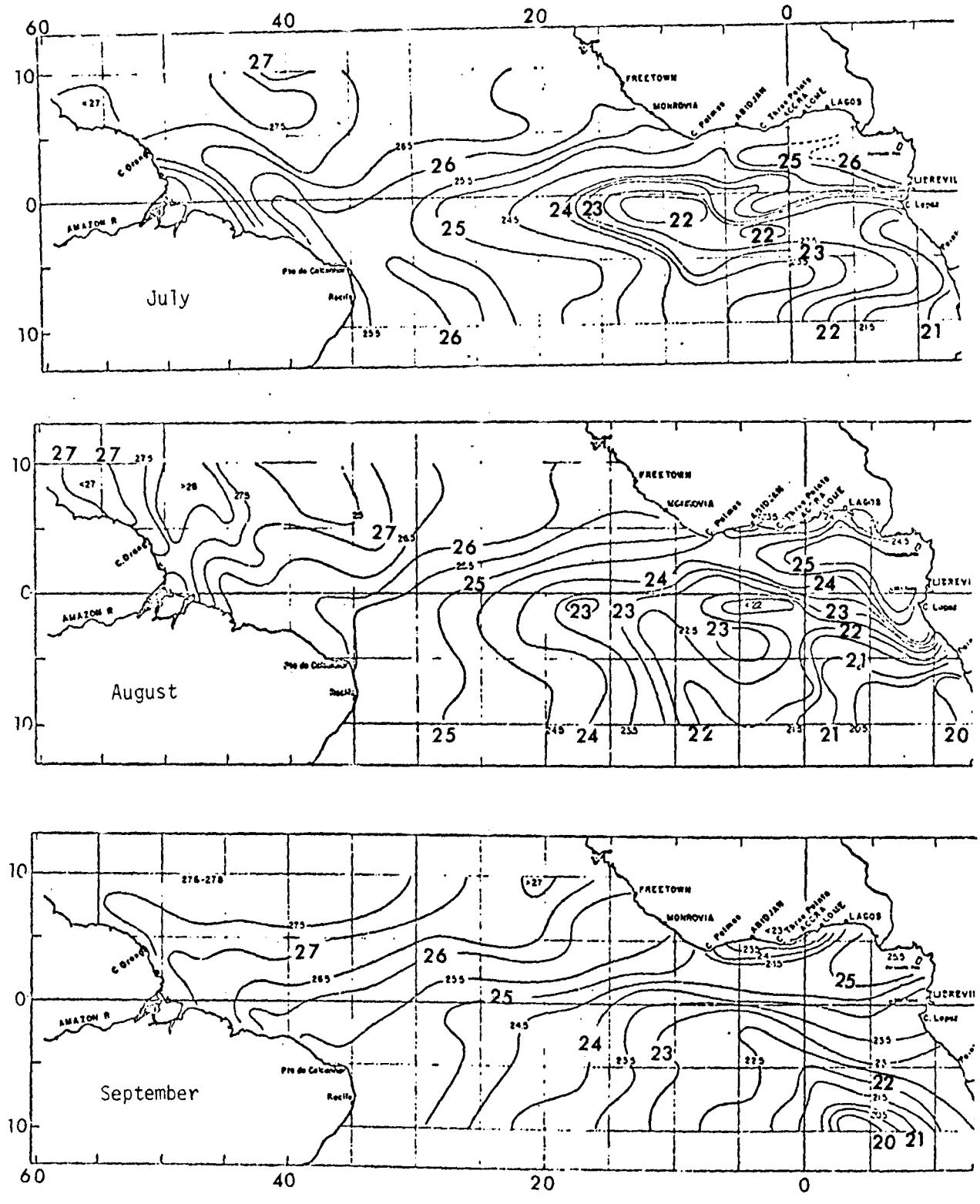

Figure 9: Same as Figure 7, except for July through September.

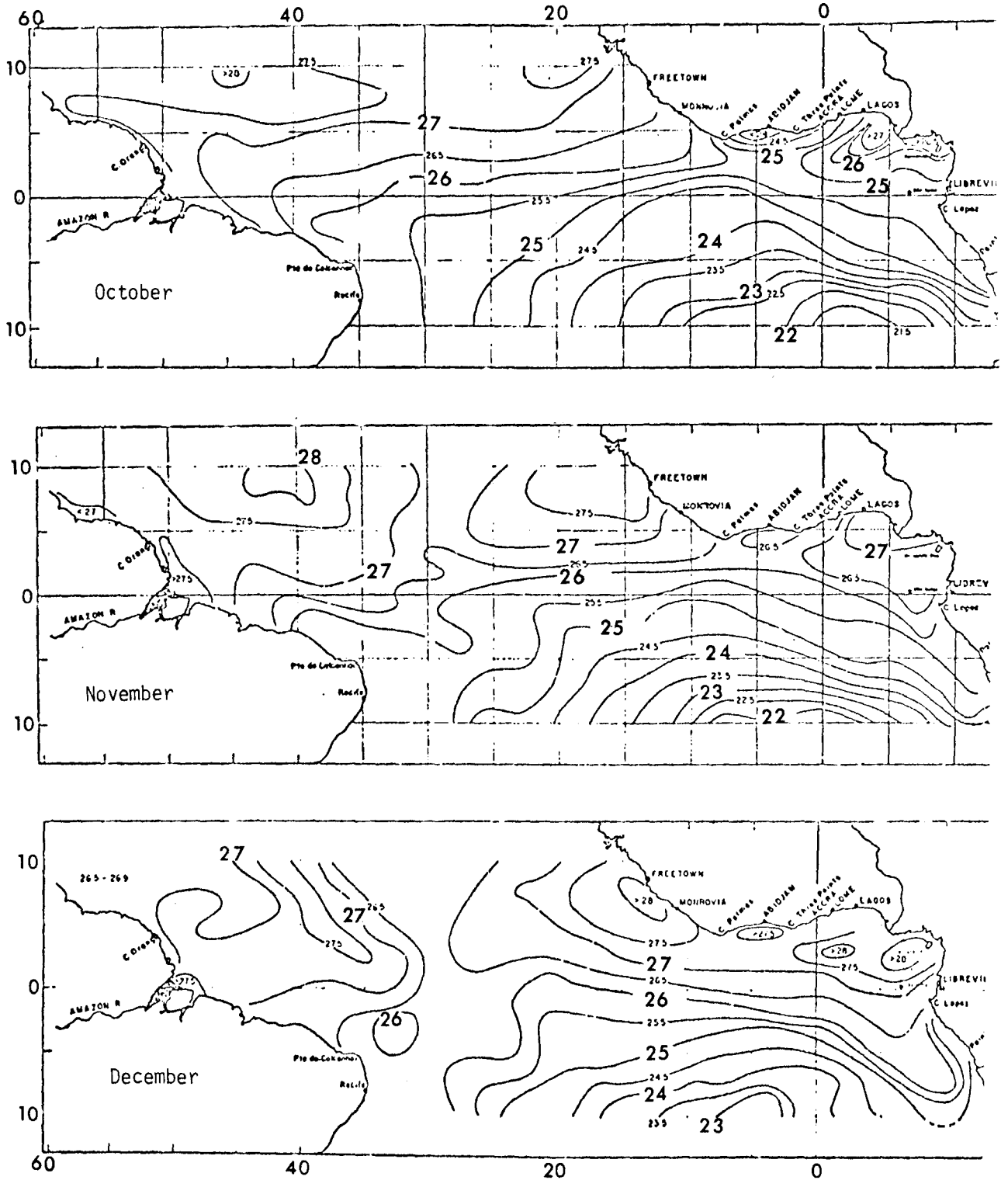

Figure 10: Same as Figure 7, except for October through December.

Table 4: Average SST (^{o}C) for the Region $25^{o}W$-$30^{o}W$, 0^{o}-$10^{o}S$.

January	26.5
February	26.5
March	27.0
April	27.5
May	27.0
June	26.5
July	25.5
August	25.0
September	25.0
October	25.0
November	25.5
December	26.0

at least 0.5°C, but its existence south of 5°S has not been documented.

The subsurface temperature field near the equator is more complicated both in time and space than the surface field. In particular, in the region of the Equatorial Undercurrent, Merle (1977) finds that at fixed depths from 50m to 150m the annual temperature range is some 6°C to 8°C. Similarly, in the region of the North Equatorial Countercurrent, the subsurface temperature structure is more variable than the surface temperature distribution (Merle, 1977). Merle's (1977) data do not extend south to the region of the South Equatorial Countercurrent.

Data collected during Equalant I and II (Kolesnikov, 1973), February-March, 1963, and August, 1963, indicate a temperature change at 1000m from about 4°C at 10°S to 4.5°C at 0°. Data from Fuglister (1960) show a 1000m temperature at 8°S somewhat lower than 4°C during March, 1957. Thus if a mean temperature of 4°C is assumed at 1000m, the vertical temperature differential, from Table 4, ranges from 21°C to 23.5°C.

Current Conditions

There are few direct measurements of the current field south of the equator in the Atlantic. Those available suggest a complicated structure of countercurrents and undercurrents present. The surface currents of the tropical Atlantic Ocean are shown schematically on Figure 11. The currents, on the average, are primarily zonal. The South Equatorial Current (SEC) is the main surface flow of the region with mean speeds of about one knot (Neumann, 1975). The SEC diverges at the tip of South America into the southerly flowing Brazil Current and northerly flowing North Brazilian Current. The intensity of the SEC in the OTEC region appears to have an annual signal, with largest speeds observed in the late spring and summer, and lowest speeds in early spring (Figure 13). In addition, the location of the split of the SEC appears to occur farther to the south along the Brazilian coast in the summer.

The discharges of OTEC operations into the SEC can become entrained downstream in the North Brazilian and/or Brazil Currents. The Brazil Current represents the western boundary current of the South Atlantic gyre, counter parts to the Gulf Stream and the North Atlantic gyre. The Brazil Current flows along the eastern coast of South America and eventually leaves the coast to flow east across the South Atlantic. The North Brazilian Current flows along the north coast of South America. A portion of this flow may become entrained in the Equatorial Undercurrent, and another portion in the North Equatorial Countercurrent (Metcalf and Stalcup, 1965, Cochrane, 1963). Some of the North Brazilian Current may enter into the Caribbean Sea to become part of the North Atlantic gyre.

The subsurface current structure is shown in Figure 13. The currents along 23.5°W were directly measured during GATE and are characterized by alternating regions of eastward and westward flow. The eastward flowing Equatorial Undercurrent (EUC) is separated from east-

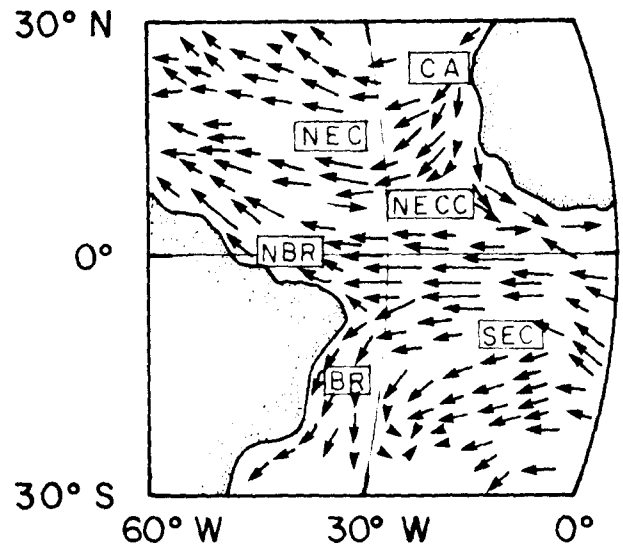

SURFACE CURRENT

BR - BRAZIL CURRENT
CA - CANARY CURRENT
NBR - NORTH BRAZILIAN CURRENT
NEC - NORTH EQUATORIAL CURRENT
NECC - NORTH EQUATORIAL COUNTER CURRENT
SEC - SOUTH EQUATORIAL CURRENT

Figure 11: A schematic representation of the currents in the tropical Atlantic, adapted from Defant (1961).

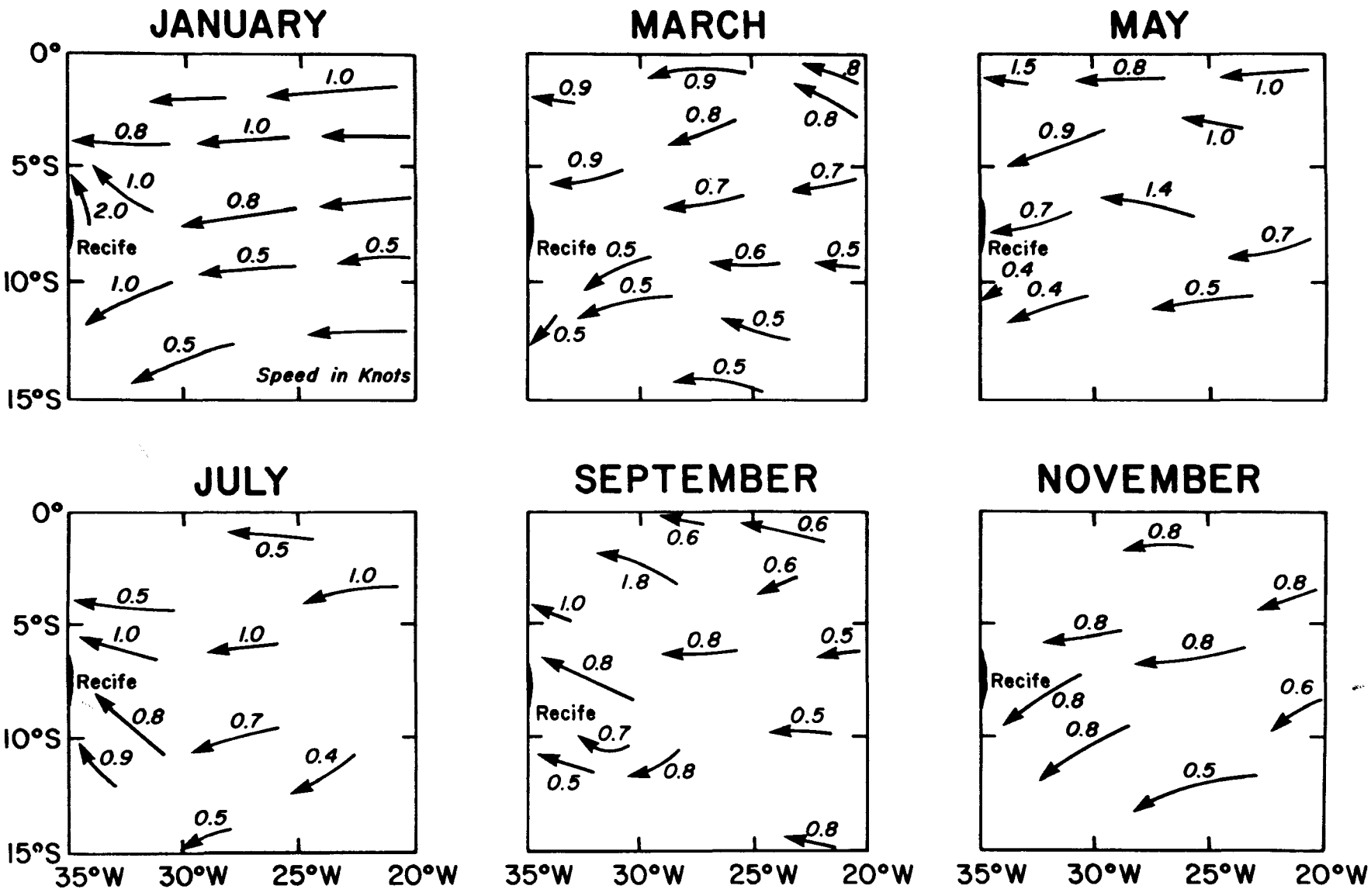

Figure 12: Surface currents in knots, deduced from ship drift reports, from Alencastro (1974).

DEPTH (m)

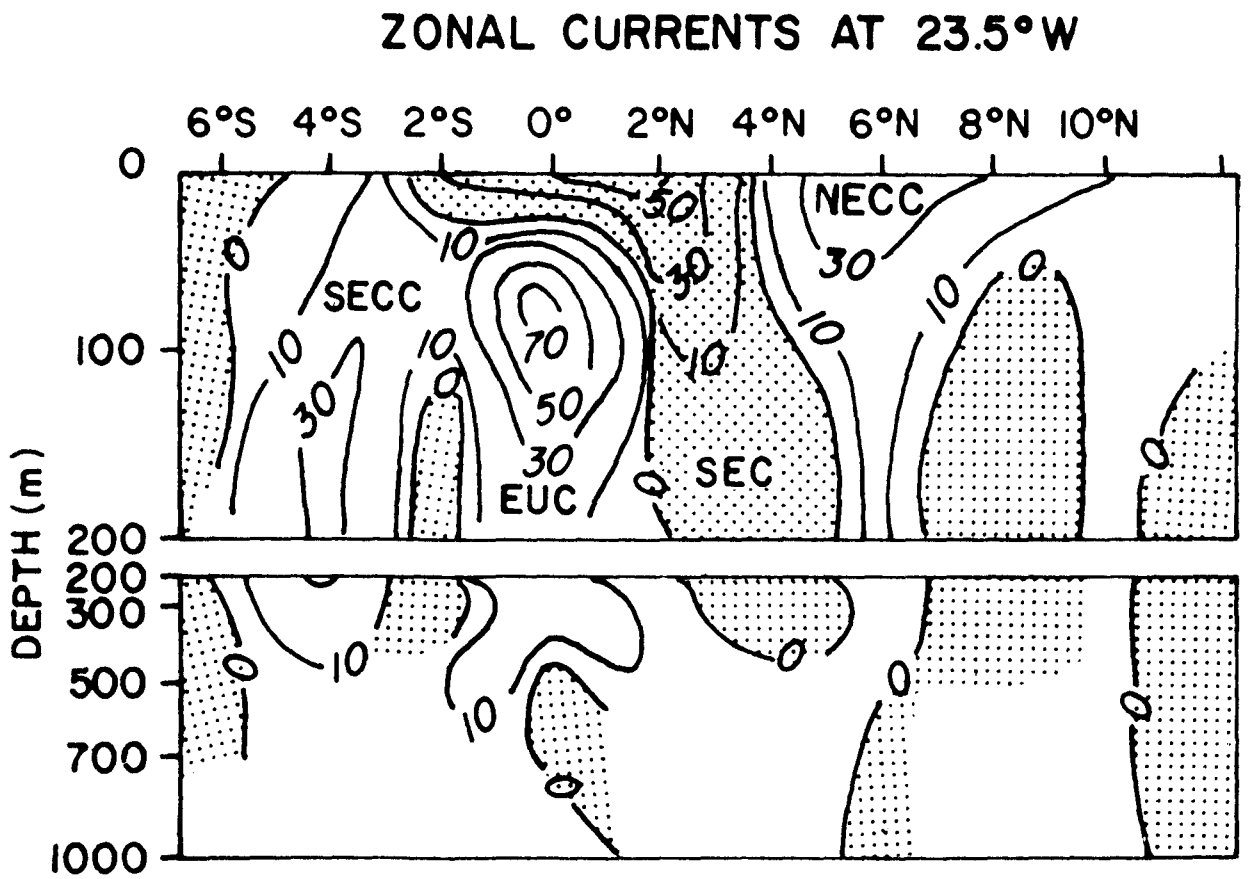

CURRENTS: SECC - SOUTH EQUATORIAL COUNTER CURRENT
EUC - EQUATORIAL UNDER CURRENT
SEC - SOUTH EQUATORIAL CURRENT
NECC - NORTH EQUATORIAL COUNTER CURRENT

CONTOURS - cm/sec

SHADED AREAS - FLOW TO THE WEST

(AFTER BUBNUV, VASILENKO AND KRIVELEVICH, 1977)

Figure 13: Directly measured currents observed during GATE, from Bubnov et al. (1977).

ward flowing North and South Equatorial Countercurrents by westward flow. The South Equatorial Countercurrent (SECC) does not appear on Neumann's charts which may be indicative of its variability at the surface. However, Merle, (1977) considered the distribution of mass in the OTEC region and found evidence for a weak SECC at the surface extending from the coast of Brazil east to at least 25°N. The SECC is found between 6°S and 10°S. Although weaker at 50m and 75m, the SECC appears again at 200m at 5°S, the southern ocean counterpart to the North Equatorial Countercurrent (NECC). South of 10°S, the westward flowing northern limb of the South Atlantic tropical gyre is located.

Additional evidence for the existence of the SECC is given by Mazeika (1968) and Cochrane (1977). Mazeika (1968) shows that velocities in the SECC can be greater than one knot at 20°W, with the current core at 150m. Cochrane (1977) computed geostrophic transport of about 20 x $10^6 m^3$/sec for the SECC.

The northern branch of the SEC is found north of the SECC, and frequently is located above the EUC. The following discussion of the EUC is given because it can serve as a sink for OTEC discharges.

Measurements of the EUC show its structure and eastward speed to be quite variable. In most of the following cases, the axis of the EUC was located between 1.5°S and 1.5°N. Philander (1973), citing Russian sources, gives speeds of 57 cm/s at 29.5°W in the fall of 1966, and 80-107 cm/s, depending on season, at 30°W. On the other hand, Stalcup et al. (1965), using drifting buoys, found speeds of about 70 cm/s in the vicinity of 25.5°W during the winter of 1963; concurrently, using moored current meters, Stalcup et al. (1965) found speeds of 60-75 cm/s at 27.5° and 30.0°W.

The variability of the Undercurrent became even more evident as improved sounding tools were available during GATE. The preliminary results of Duing (1975) summarized below, illustrates the variability:

(a) Maximum eastward speed in the core varied from 65 cm/s on 26 July to 175 cm/s on 4 August;

(b) eastward volume transport varied from 4 x $10^6 m^3$/s on 27 July to 15 x $10^6 m^3$/s on 5 August

(c) at first the eastward core moved from near 1°S to 1°N, it then moved south and back across the equator;

(d) on 10 August the Undercurrent surfaced at 1.5°S, by 15 August eastward flow extended some 60km farther north;

(e) the data suggest a westward wave propagation with phase speed of 157 cm/s and a period of 18 days.

There is little direct data on the temporal variability of other currents in the region. However, some inferences can be made from theoretical considerations as discussed in the next section.

Theoretical Studies

The cause of the Equatorial Undercurrent (EUC) in some linear theories (Gill, 1975) is the pressure gradient established along the equator by the overlying wind field. At the equator, the Coriolis force is zero so geostrophic currents can not exist. The westward Trades pile up lighter surface waters on the western side of the ocean, which establishes a pressure gradient along the equator from west to east. The eastward flowing Undercurrent is a response to this pressure gradient. In addition, a meriodional circulation is established just off the equator through an Ekman drift. North of the equator, at the surface, the Ekman drift is to the north, and conversely, south of the equator to the south. To compensate for this surface drift, deeper equatorward flows adds transport to the Undercurrent at the thermocline. These meriodional motions could serve to transport OTEC discharges from further south into the EUC.

Philander (1973) notes that the Equatorial Undercurrent (EUC) appears to be very sensitive to changes in the local wind stress. During weak winds, (September through January), the EUC is characterized by a strong narrow flow which is symmetric about the equator. During these times the thermocline weakens and spreads in the vertical. When the trades stop (February through April), the EUC can surface, and the upper layer isotherms ridge but the deeper isotherms do not dip. Finally, when the SE trades are strongest, there is an intense westerly surface flow, but a weak EUC. However, it is also possible that these features of the EUC are related to the long-term wind-stress average, rather than the local curl. It is interesting to note that each phase of the EUC is characterized by a different upper layer thermal structure. Gill (1975) notes that the EUC may also be thermally driven.

In addition to these long-term trends, short-term variability in the thermal and current fields has been observed. Because the equator acts as a wave-guide, this variability has been attributed to wave motions induced by atmospheric features with similar period (Hallock (1977), for instance).

The South Equatorial Current has a north and south branch which are separated at least part of the time by a South Equatorial Counter Current. The SEC is the northern branch of the South Atlantic gyre and as such is driven largely by the curl of the wind stress over this basin.

If the SECC is dynamically the southern counterpart of the North Equatorial Countercurrent, then it may be related to the position of the Doldrums relative to the equator. Figure 14, from Neumann and Pierson

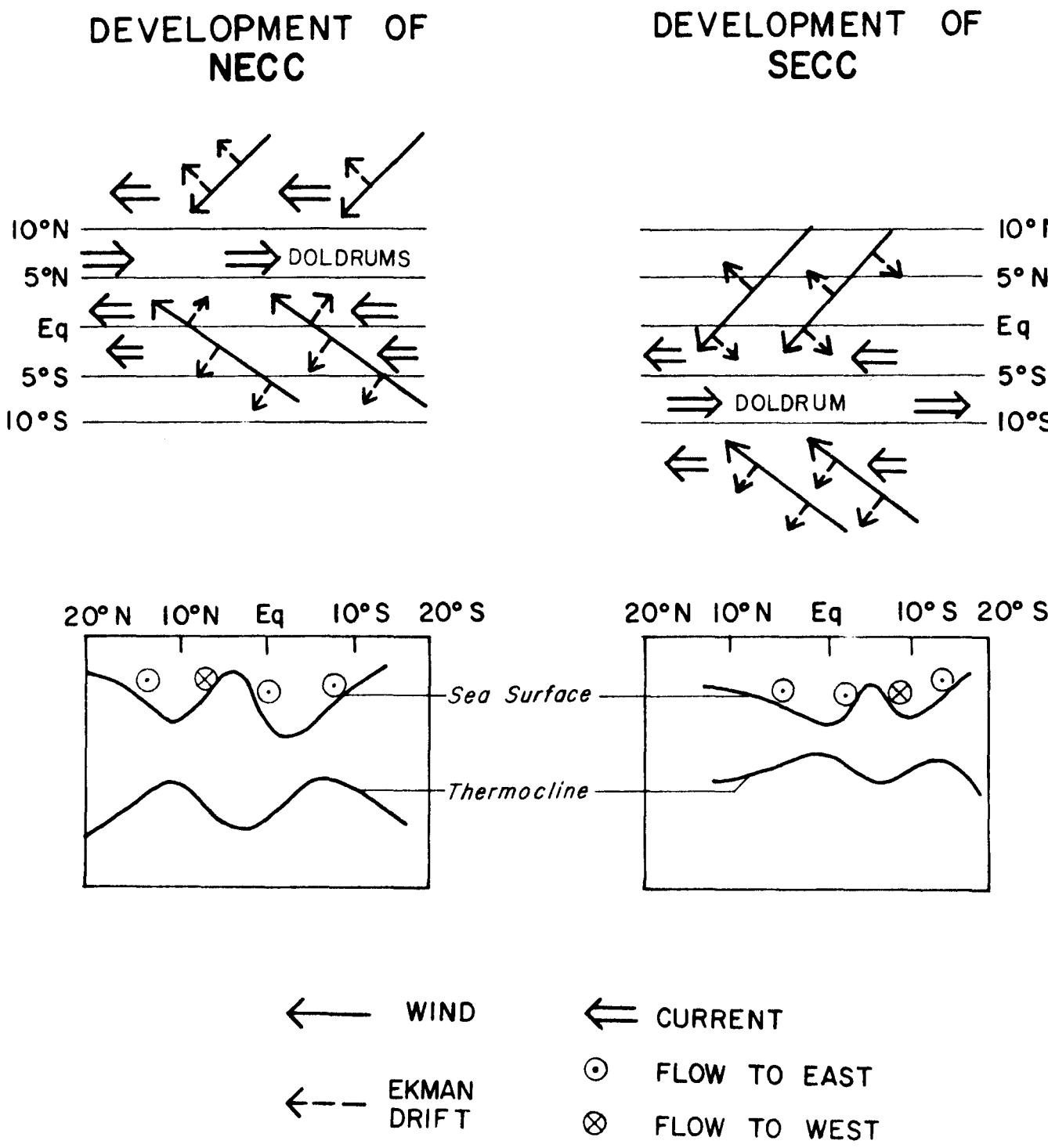

Figure 14: The relation of the sea surface winds to the North and South Equatorial Countercurrents, from Neumann and Pierson (1966).

(1966), indicates that when the ITCZ is south of the equator a SECC should exist. Because the ITCZ is south of the equator only a few months out of the year, the SECC may be a more variable feature than the NECC.

Several recent papers suggest that poleward of 5^{o} to 7^{o} in either hemisphere the thermal field responds to changes in the local curl of the wind stress. Meyers (1975) found that the vertical movement of the thermocline was related to the variability in the curl of the local wind stress. His study was in the Pacific, and the variability in the thermal field was mirrored by changes in the current field. That is, the annual cycle of the transport of the NECC in the Pacific is in phase with these changes in the wind and temperature fields. However, White (1976) found that Rossby waves generated at the eastern boundary causes thermal variability. Thus, in the view of White (1976), local thermal changes are induced by a combination of Rossby wave and local curl forcing. In either case, the structure and variability of the wind field over the OTEC area could produce changes in the thermal and current structure similar to those observed by White (1976) and Meyers (1975).

IV. Climatological Data Representations

The historical data-set available in the tropical South Atlantic is quite limited. Therefore, it was necessary to average over large intervals both in time and space in order to generate charts representing climatological conditions. The temporal averaging interval is three months and the seasons are January-March, April-June, July-September, and October-December. The spatial averaging interval is 1^{o} latitude by 5^{o} longitude quadrangles. Because the currents in the area appear, on the average, to be zonal, a larger averaging interval in the east-west direction should increase the data available in each quadrangle, without the penalty of increasing the spatial variability within the quadrangle. The grid established for the climatological representations is shown on Figure 15.

Seasonal temperature-versus-depth plots for the quadrangles between $25^{o}W$ and $30^{o}W$ are shown in Figure 16. Table 5 lists the number of data points and standard deviations for those quandrangles with greater than five data values. The means and standard deviations were computed from Nansen, MBT, and XBT data. However, the fact that only one quadrangle (not shown) had more than five values below 250m indicates that most of the data were from MBT's. In addition, the large number of values during January-March and July-September indicate that a majority of the data were collected during Equalant I and II (Kolesnikov, 1973), an international investigation of the tropical Atlantic Ocean conducted in February-March 1963 and August 1963. Thus, the profiles of Figure 16 and the horizontal distributions to be presented probably give a realization of the average conditions and variability in the region biased by these periods.

The seasonal cycle of surface heating is evident in each quadrangle, with warmest temperatures observed in January through March, and coldest

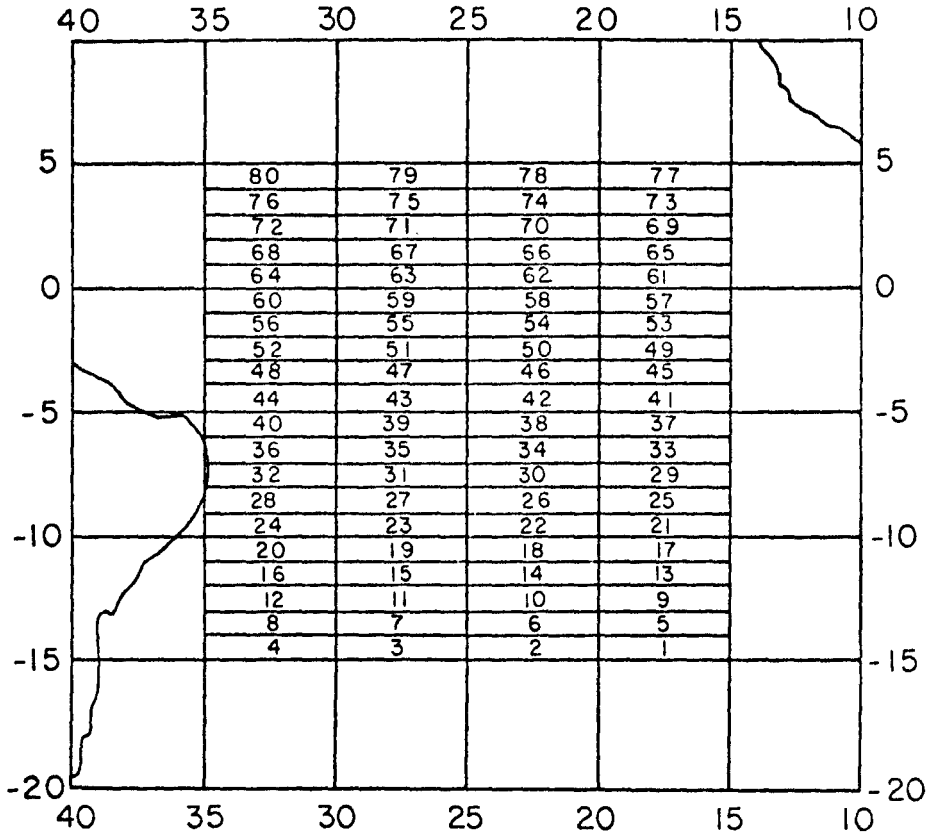

One by five degree: area index codes (NODC)

Figure 15: Subregions used to generate horizontal distribution maps.

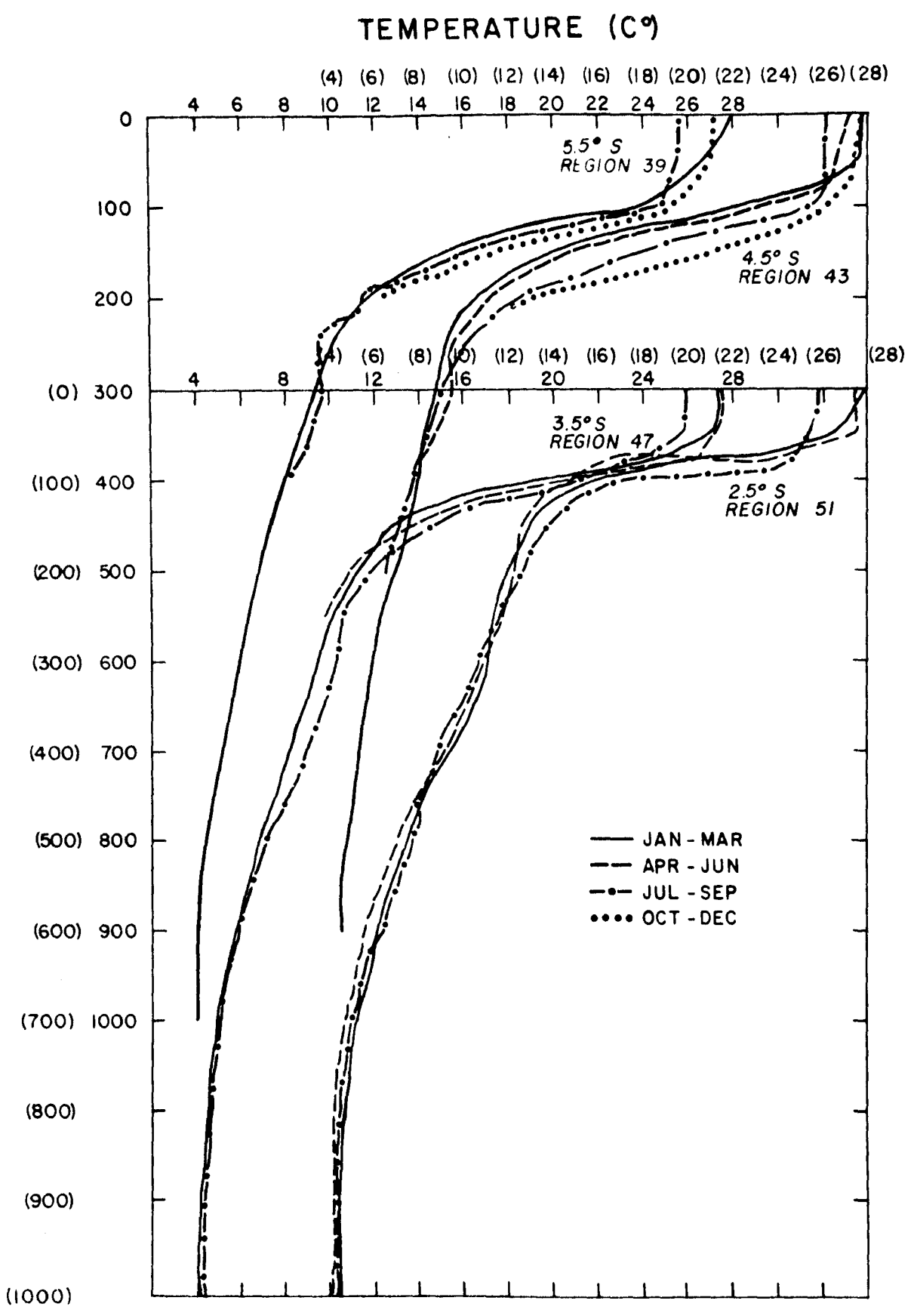

Figure 16: Average temperature profiles for the subregions between 25°W and 30°W (Figure 15) by season.

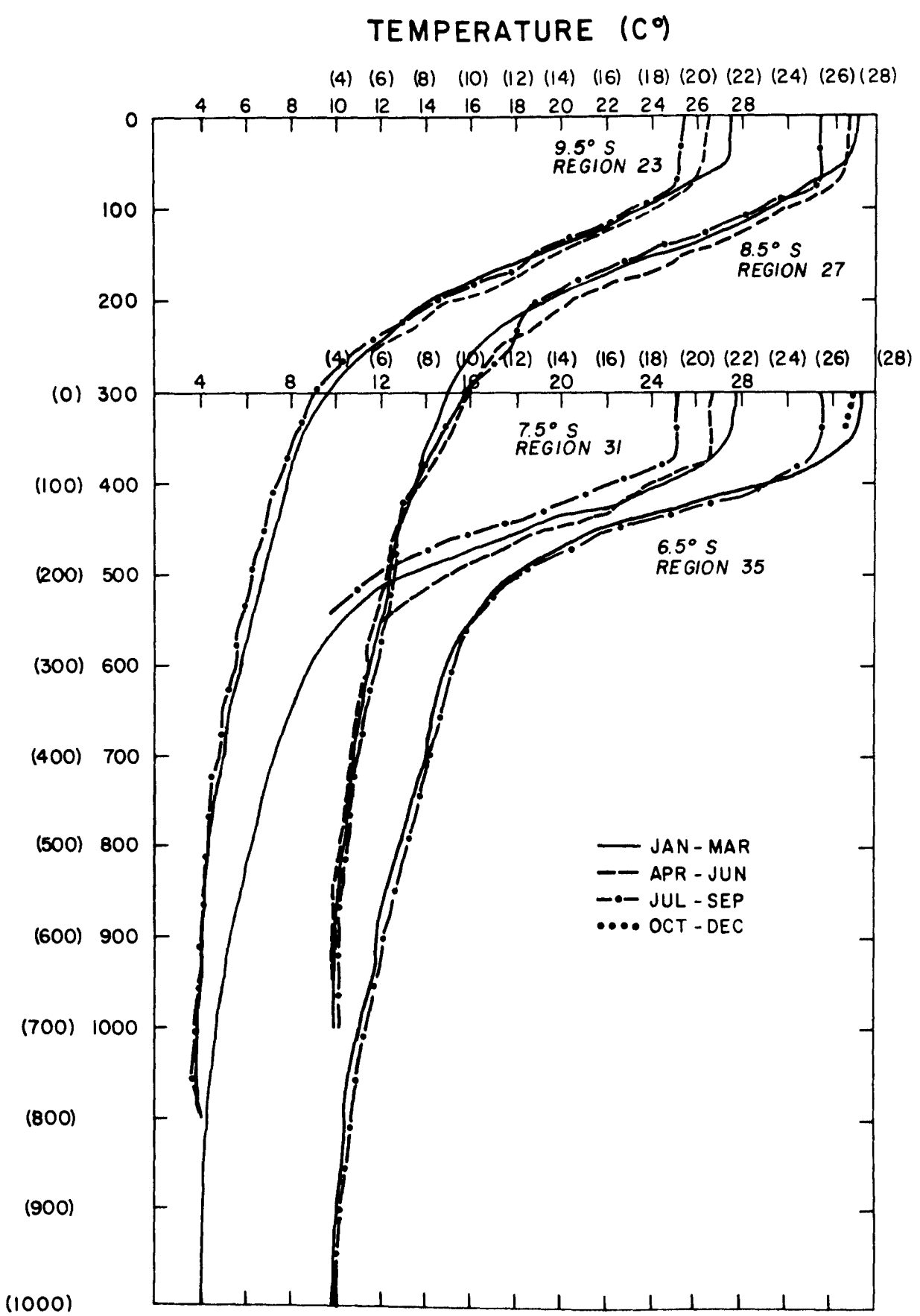

Figure 16: continued

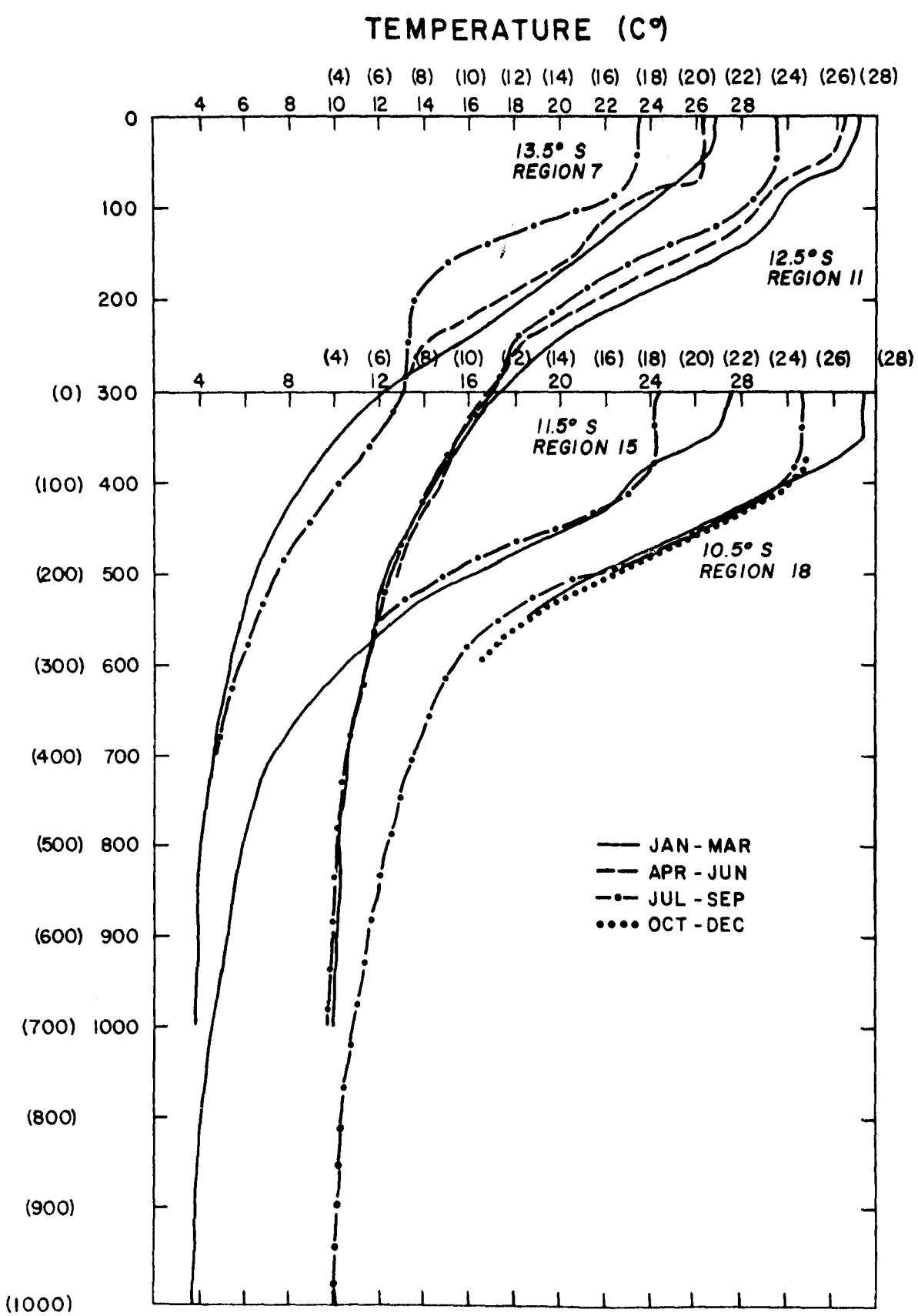

Figure 16: continued

TABLE 5: Number of data points N, and standard deviations, S. D., for those quadrangles between 25°W and 30°W with more than five data values.

Latitude	13.5°S	12.5°S	11.5°S	11.5°S	10.5°S	10.5°S	9.5°S	9.5°S	9.5°S
Quadrangle	7	11	15	15	19	19	23	23	23
Season	Jan-Mar	Jan-Mar	Jan-Mar	Jul-Sep	Jan-Mar	Jul-Sep	Jan-Mar	Apr-Jun	Jul-Sep
	N/S.D.	N/S.D.	N/S.D.	N/S.D.	N/S.D.	N/S.D.	N/S.D.	N/S.D.	N/S.D.
0	24/ .59	10/ .71	24/ .47	5/ .47	12/ .21	7/ .43	14/ .58	16/ .24	10/ .95
10	24/ .57	10/ .68	24/ .44	5/ .47	12/ .21	7/ .42	14/ .54	16/ .24	10/ .99
20	24/ .52	10/ .64	24/ .43	5/ .45	12/ .20	7/ .41	14/ .51	16/ .24	10/1.02
30	24/ .46	10/ .67	24/ .44	5/ .44	12/ .20	7/ .40	14/ .51	16/ .24	10/1.04
50	24/ .46	10/ .77	24/ .53	5/ .42	12/ .23	7/ .37	14/ .56	16/ .26	10/1.09
75	24/ .51	9/ .30	24/ .34	5/ .40	12/ .84	7/ .26	14/ .93	16/ .62	10/1.19
100	24/ .39	9/ .29	24/ .40	5/ .62	12/ .36	7/ .54	14/ .59	16/ .58	10/1.84
125	24/ .48	9/ .53	24/ .68		12/ .49	7/1.05	14/1.01	16/ .66	10/1.93
150	24/ .78	9/1.30	24/1.08		12/ .83	6/ .95	14/1.13	16/ .59	8/1.47
200	24/1.12	9/1.09	24/ .73		10/ .34	6/ .58	12/ .89	16/ .50	8/1.08
250	16/ .53								6/ .51

Latitude	8.5°S	8.5°S	8.5°S	7.5°S	6.5°S	6.5°S	5.5°S	5.5°S	5.5°S
Quadrangle	27	27	27	31	35	35	39	39	39
Season	Jan-Mar	Apr-Jun	Jul-Sep	Jan-Mar	Jan-Mar	Oct-Dec	Jan-Mar	Jul-Sep	Oct-Dec
0	39/ .22	24/ .30	9/1.00	36/ .50	8/ .21	9/ .04	9/ .69	5/ .78	7/ .18
10	39/ .21	22/ .20	9/1.00	36/ .47	8/ .21	9/ .03	9/ .65	5/ .76	7/ .16
20	39/ .20	22/ .20	9/1.00	36/ .46	8/ .22	9/ .03	9/ .65	5/ .79	7/ .16
30	39/ .22	22/ .19	9/1.01	36/ .48	8/ .21	9/ .04	9/ .61	5/ .80	7/ .12
50	39/ .43	22/ .21	9/1.00	36/ .52	8/ .27	9/ .06	9/ .61	5/ .72	7/ .12
75	38/ .53	22/ .35	9/1.06	35/ .67	8/ .39	9/ .26	9/ .41	5/ .44	7/ .10
100	38/ .43	22/ .49	9/1.03	35/ .67	8/ .58	9/ .71	9/1.03	5/ .90	7/ .56
125	38/1.19	22/ .42	9/1.44	35/1.17	8/ .68	9/ .55	9/ .73		7/ .76
150	38/1.42	22/ .61	9/1.54	35/1.01	8/ .80	9/ .29	9/ .80		7/ .90
200	38/ .98	22/ .59	9/1.30	28/ .63	8/ .48	9/ .33	9/ .46		7/ .38
250	13/ .64		6/ .87	12/ .30			6/ .52		

Latitude	4.5°S	4.5°S	4.5°S	4.5°S	3.5°S	3.5°S	3.5°S
Quadrangle	43	43	43	43	47	47	47
Season	Jan-Mar	Apr-Jun	Jul-Sep	Oct-Dec	Jan-Mar	Apr-Jun	Jul-Aug
0	24/ .45	9/ .43	13/ .95	7/ .09	24/ .53	21/ .23	10/1.24
10	24/ .44	8/ .20	13/ .95	7/ .09	24/ .53	21/ .17	10/1.22
20	24/ .40	8/ .24	13/ .95	7/ .09	24/ .52	21/ .16	10/1.22
30	24/ .39	8/ .51	13/ .95	7/ .08	24/ .48	21/ .16	10/1.21
50	24/ .39	8/1.10	13/ .93	7/ .09	23/ .45	21/ .16	10/1.26
75	23/ .44	8/1.78	13/ .90	7/ .27	23/1.15	21/ .83	10/2.78
100	23/1.22	8/1.49	13/ .73	7/ .57	23/2.27	21/2.52	10/4.55
125	23/1.23	8/ .56	13/2.23	7/ .71	23/1.51	21/1.91	10/3.16
150	23/ .78	8/ .64	10/1.71	7/ .58	23/ .72	21/ .91	10/1.73
200	23/ .40	8/ .87	10/ .98	7/ .43	23/ .55	21/ .33	8/ .53
250	15/ .32	8/ .64	10/ .70		13/ .86	20/ .57	8/ .83

in July through September (Figure 16). The average annual variability in sea-surface temperature (SST) over the entire ATL-1 region is approximately .5°C. There does not appear to be a consistent north-south change in the variability of the SST. However, on the average the largest variability in SST appears to occur in the summer. It should be remembered, however, that the data-set is quite limited in coverage.

The largest variability in the vertical occurs near the depth of the thermocline. This depth varies from 150m to 200m in the south to 100m to 125m in the north. The variability in temperature at the depths of the thermocline is greater than 1°C.

Horizontal plots of the seasonal distributional of several thermal variables also were produced. The distribution of SST is shown on Figure 17. From January through March, the SST in ATL-1 ranges from 27.5°C to 28°C, while from July through September the range is 25°C to 26°C. The warmest SST temperatures between 25°W and 30°W most often occur between 3°S and 10°S; and possibly in the western portions of the longitudinal band. South of 10°S, reduced SST is observed in all seasons.

The 900m and 1000m temperature distributions are shown on Figures 18 and 19, respectively. There is little difference between these two distributions. The temperature increases at 900m from about 4.2° at 10°S to about 4.6°C at the equator during all seasons. The range at 1000m is from about 4.0°C to 4.4°C.

Only the temperature difference between the sea-surface and 900m is shown (Figure 20), because of the similarity between the temperature distributions at 900m and 1000m. The distributions of temperature difference are very similar to the SST distributions, as the temperature gradient at 900m is small. As in the case of SST, on the average the largest temperature differences occur between 3°S and 10°S, and to the west of the ATL-1 region. The thermal resource in the ATL-1 area is between 21°C and 22°C during July through September and between 23.5°C and 24°C during January through March.

The mixed layer depth (MLD) is defined as the depth to the center of the first depth interval in which the temperature changes by 0.3°C. The deepest MLD's occur from July through September and are of the order of 80m (Figure 21). The shallowest MLD's occur from January through March and are of the order of 50m. The seasonal variability of the MLD is consistent with winter cooling and summer heating of the upper layer. The MLD becomes more shallow (about 20m) from north to south during most seasons.

The thermocline depth is defined as the first 10-meter depth interval over which the temperature changes 0.5°C The seasonal distributions of the depth of the thermocline are shown on Figure 22. In the ATL-1 region, the thermocline depth ranges from about 100m to 140m. The shallowest thermoclines are generally found in the northern part of the region, with a general deepening trend to the south. The range in thermocline depths from about 5°S to 10°S in the ATL-1 area, is on the average, about 20m.

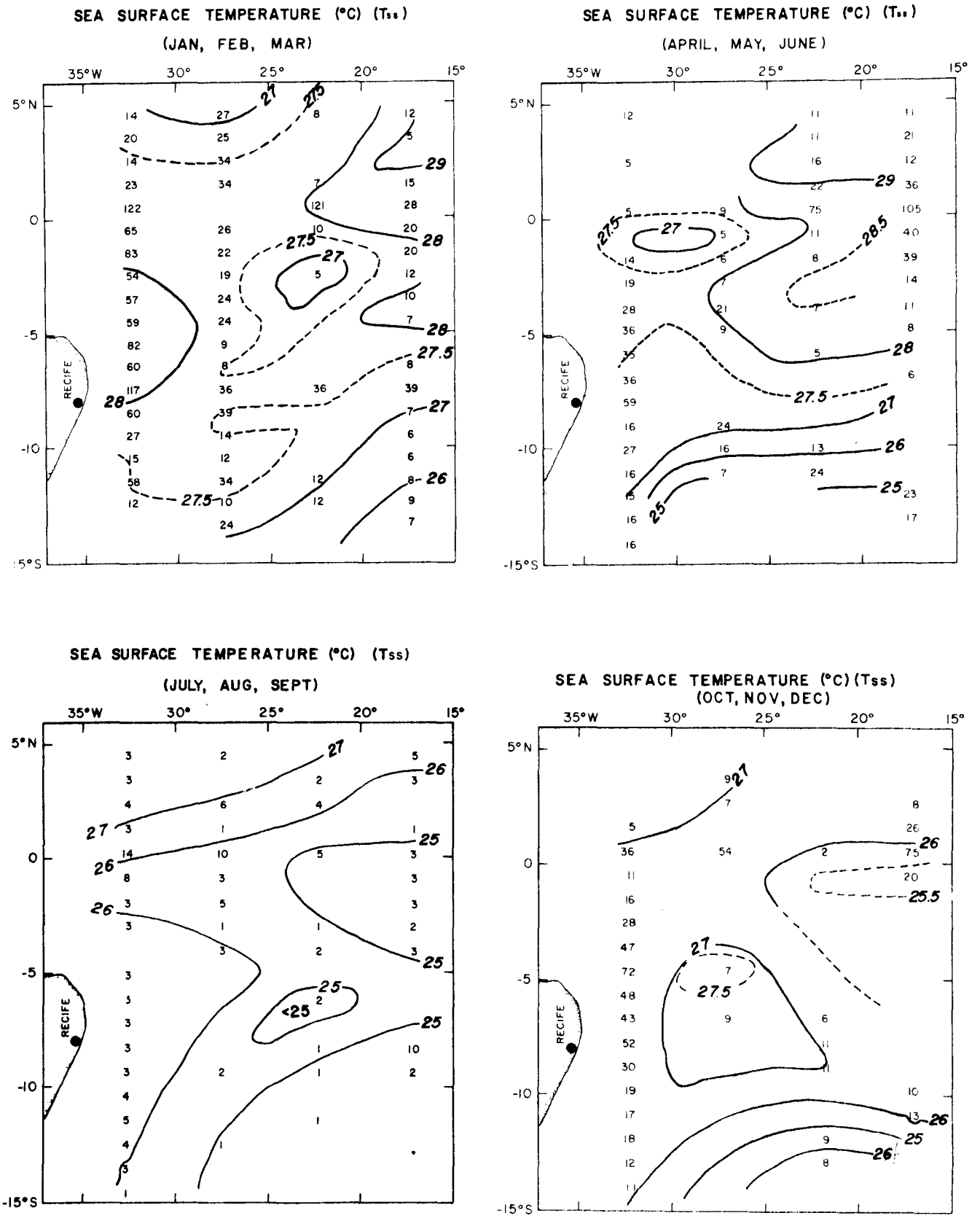

Figure 17: Mean seasonal distributions of sea surface temperature (^{o}C). at 900 m. The number of data points available in each sub-region is also shown.

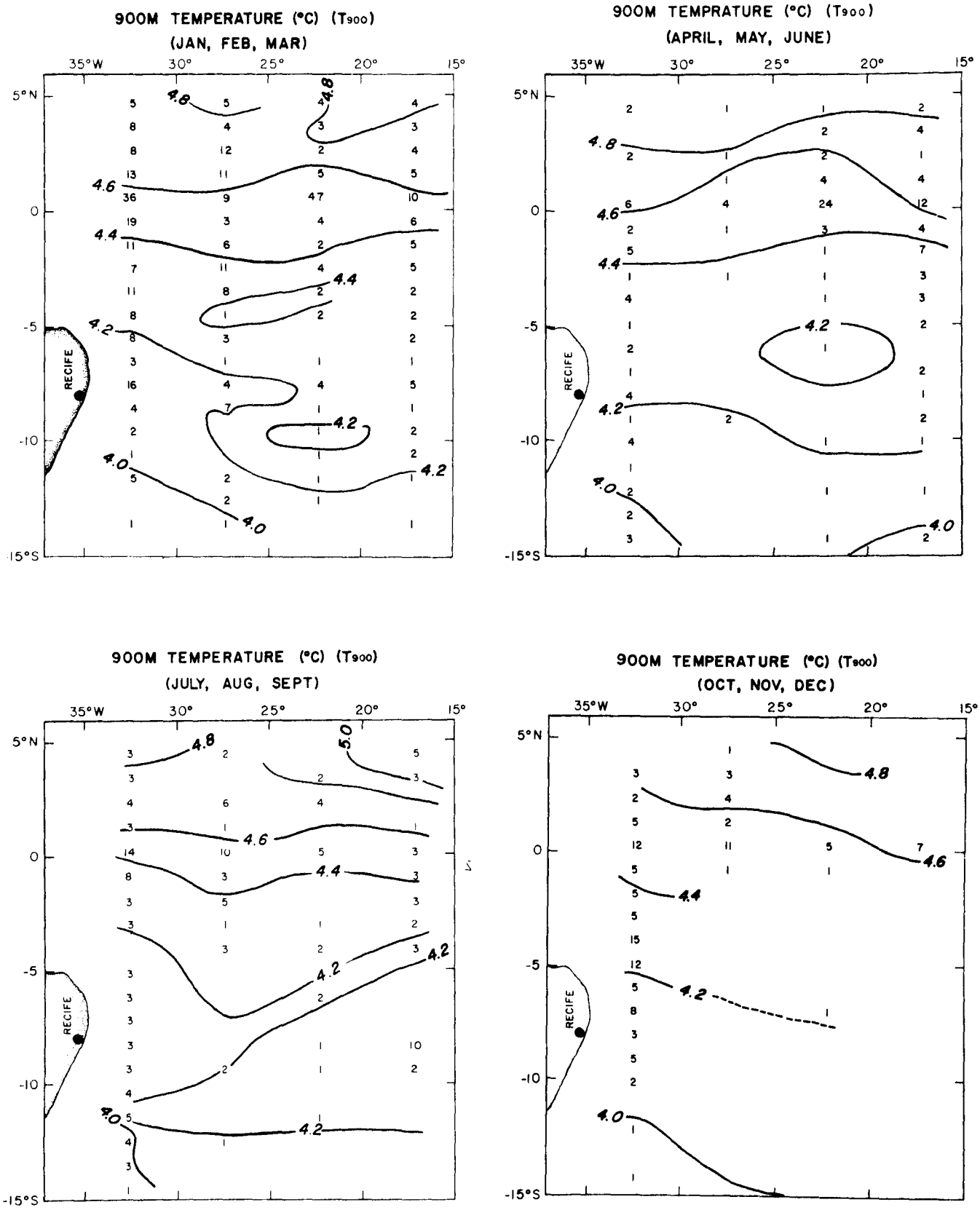

Figure 18: Mean seasonal distributions of temperature (^{o}C) at 900 m. The number of data points available in each subregion is also shown.

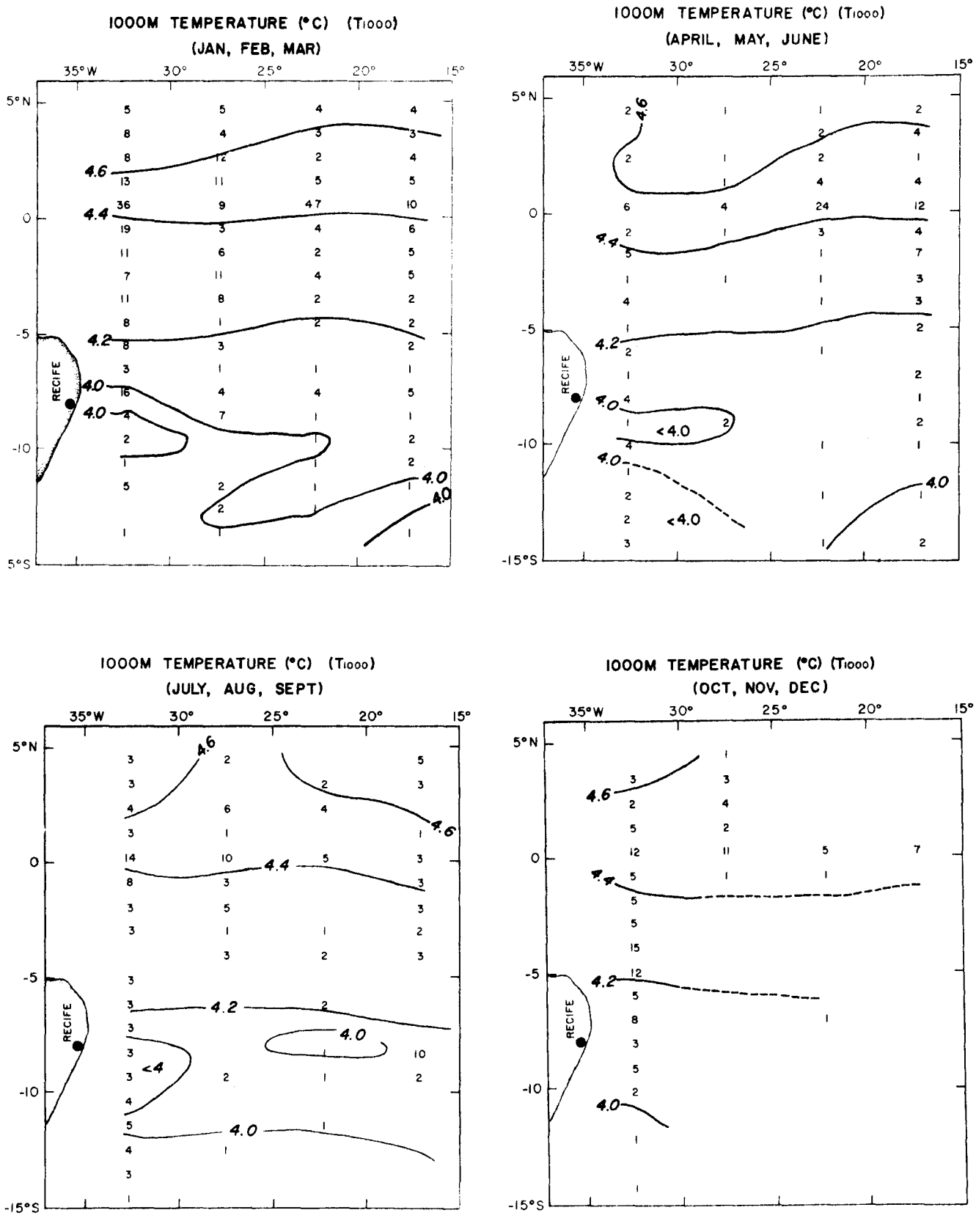

Figure 19: Mean seasonal distributions of temperature (°C) at 1000 m. The number of data points available in each subregion is also shown.

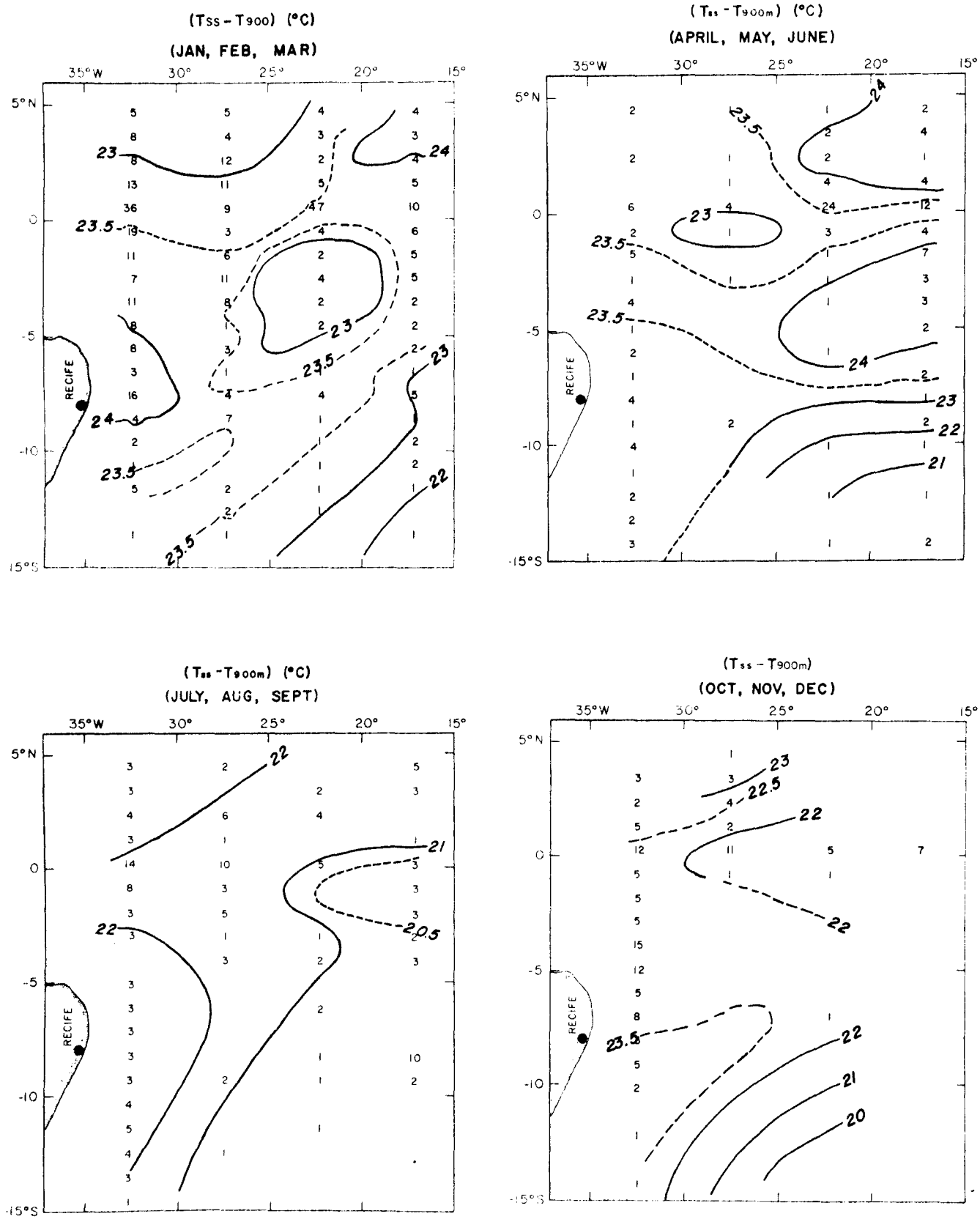

Figure 20: Mean seasonal distributions of temperature differences between the sea surface and 900 m (°C). The number of data points available in each subregion is also shown.

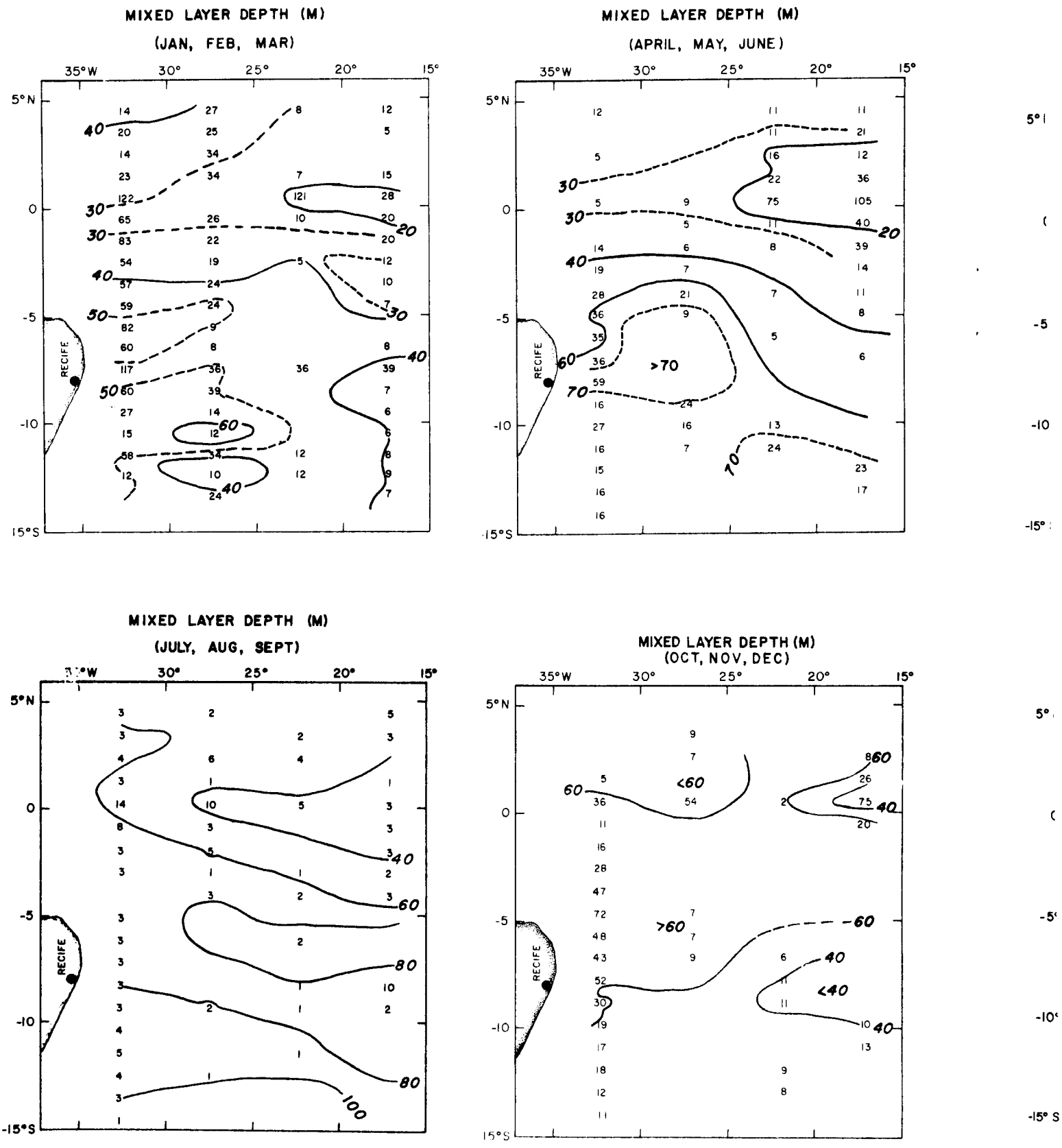

Figure 21: Mean seasonal distributions of mixed layer depth (m). The number of data points available in each subregion is also shown.

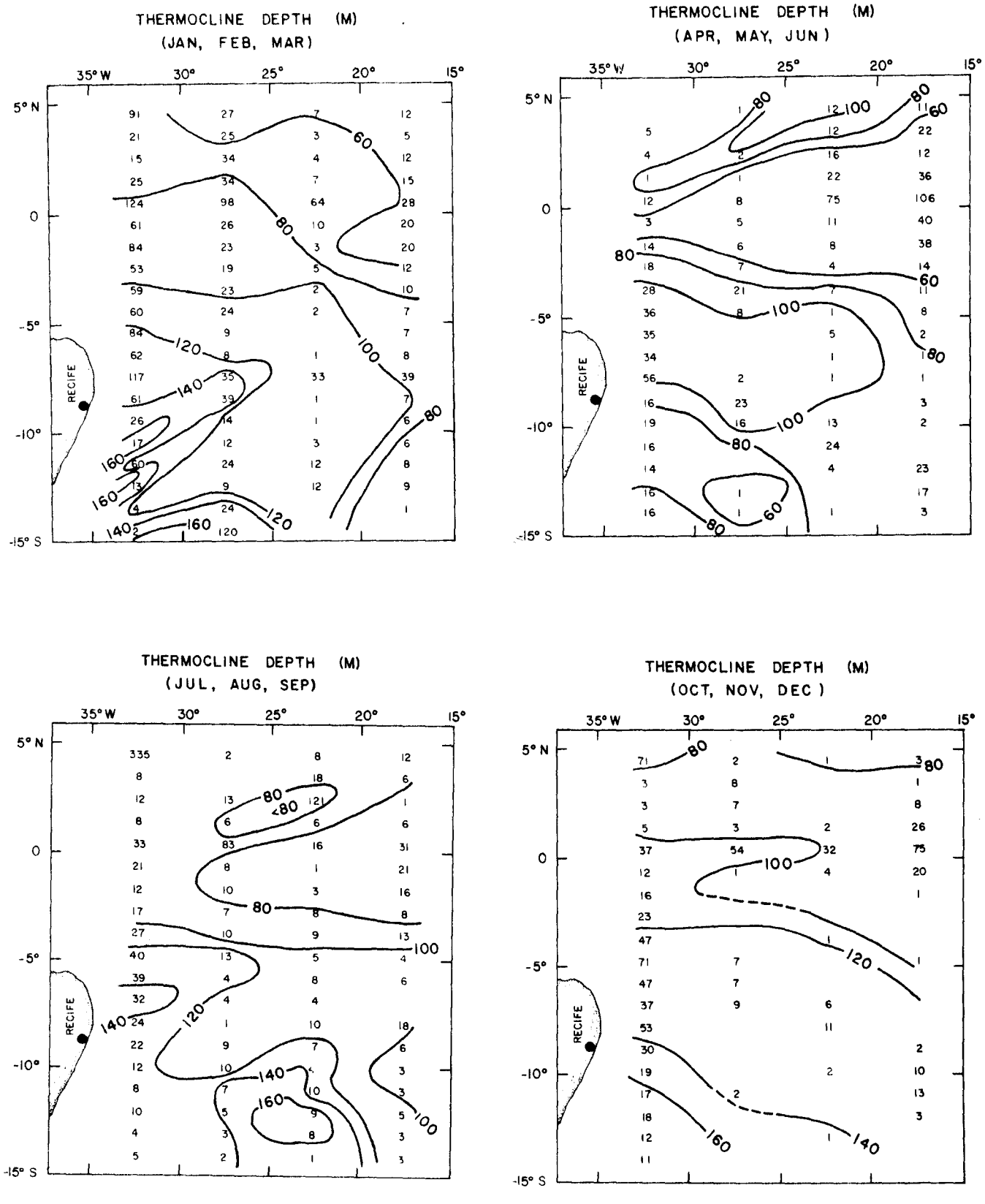

Figure 22: Mean seasonal distributions of thermocline depth (m). The number of data points available in each subregion is also shown.

V. Synoptic Data Representations

Prior to GATE, there was only one large-scale experiment to study the environmental conditions in the South Atlantic. Therefore, few data-sets exist which portray the synoptic thermal and current distributions at ATL-1. However, some indication of the spatial variability on the time-scales less than seasonal can be obtained from the few existing data-sets.

The SST distributions observed during Equalant I and II are shown on Figure 23 (from Kolesnilsov, 1973). During both seasons, the range of SST in the ATL-1 region is of the order 1°C. However, it should be noted that the data were obtained on widely separated sections. SST data collected in the NW corner of the ATL-1, Figure 23, from Alencastro (1972) also indicate a 1°C range in SST. Once again the sections are widely separated in space and indicate no significant fronts exist in the SST distribution.

Longitudinal sections of temperature obtained during Equalant I and II are shown on Figures 24 and 25, respectively. The distribution of SST along some of these lines also is shown on these figures. The temperature sections have several similar properties. The thermocline rises dramatically at 4°S during Equalant I, and at about 5.5°S during Equalant II. In addition, the temperature gradient at the thermocline increases at these locations. The SST distribution along 25°W suggests that the range of SST was somewhat larger in August 1963 than in February-March 1963. The zonal temperature sections shown on Figure 26 indicate small slopes in the isotherms along several latitude lines.

Additional synoptic data were collected in the South Atlantic during GATE. A summary of the verbal presentations made during the GATE symposium, May, 1977, which are pertinent to ATL-1 is given in Appendix 2. A list of those data collected in the South Atlantic during GATE are also included. These data have been requested from World Data Center-A and will be analyzed for inclusion in the final report on the physical characteristics of ATL-1.

VI. Summary

The lack of sufficient data precludes any quantitative statements about the time and space scales of the temperature and current distributions in the the ATL-1 region. Estimates of the mean thermal properties and a qualitative measure of their variability are summarized in Table 6. It should be stressed again that these mean values are computed primarily from the Equalant data, so they are heavily biased by measurements made in February, March and August 1963. Further analysis is required to determine what portion of the variability is caused either by the large spatial averaging interval, by the three-month temporal averaging interval, or by interannual variability.

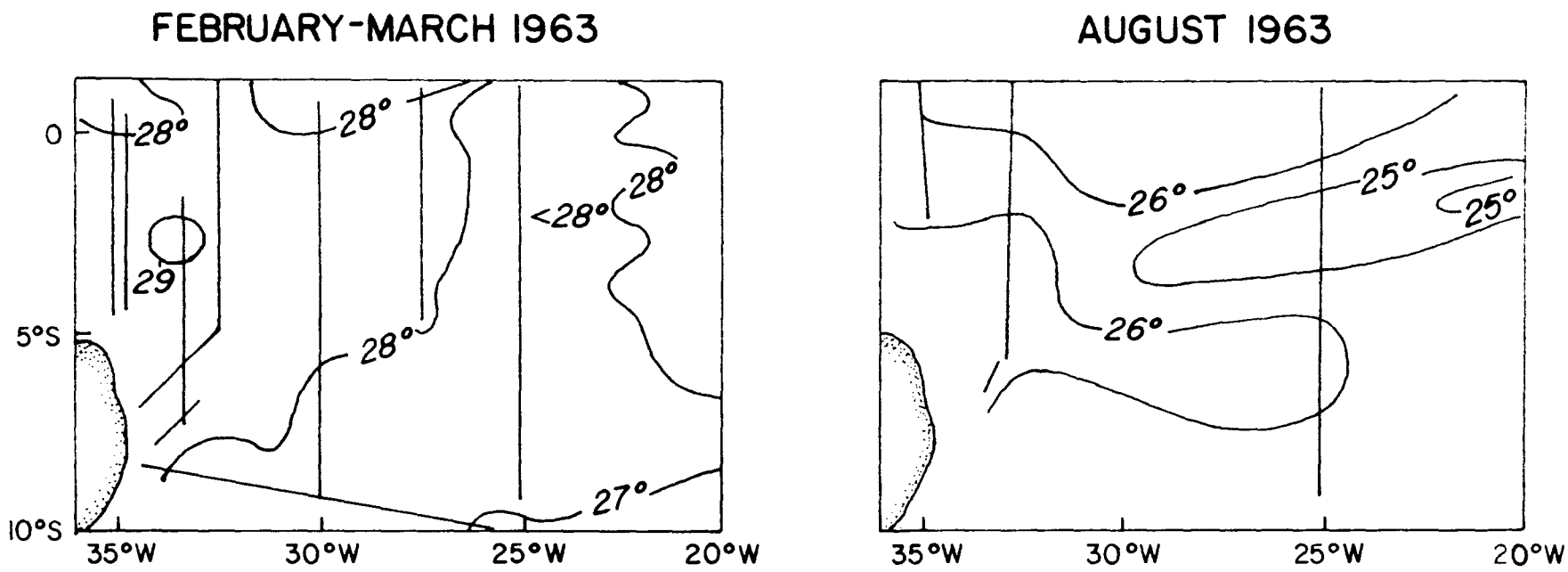

Figure 23: Sea surface temperatures (^{o}C) observed during Equalant (Kolesnikov, 1973), and September - October, 1971 (Alencastro, 1972).

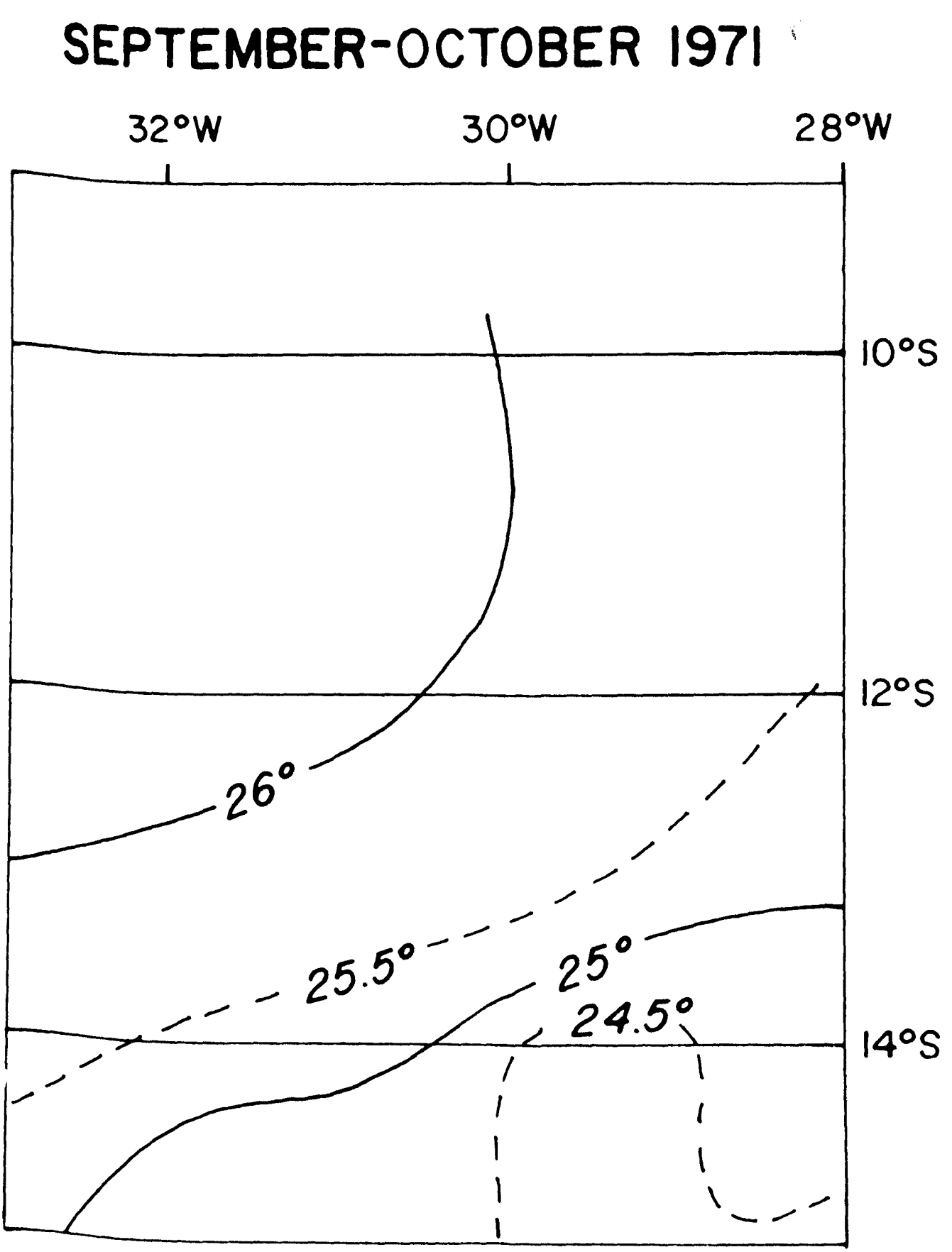

FEBRUARY-MARCH 1963

Figure 23: Continued

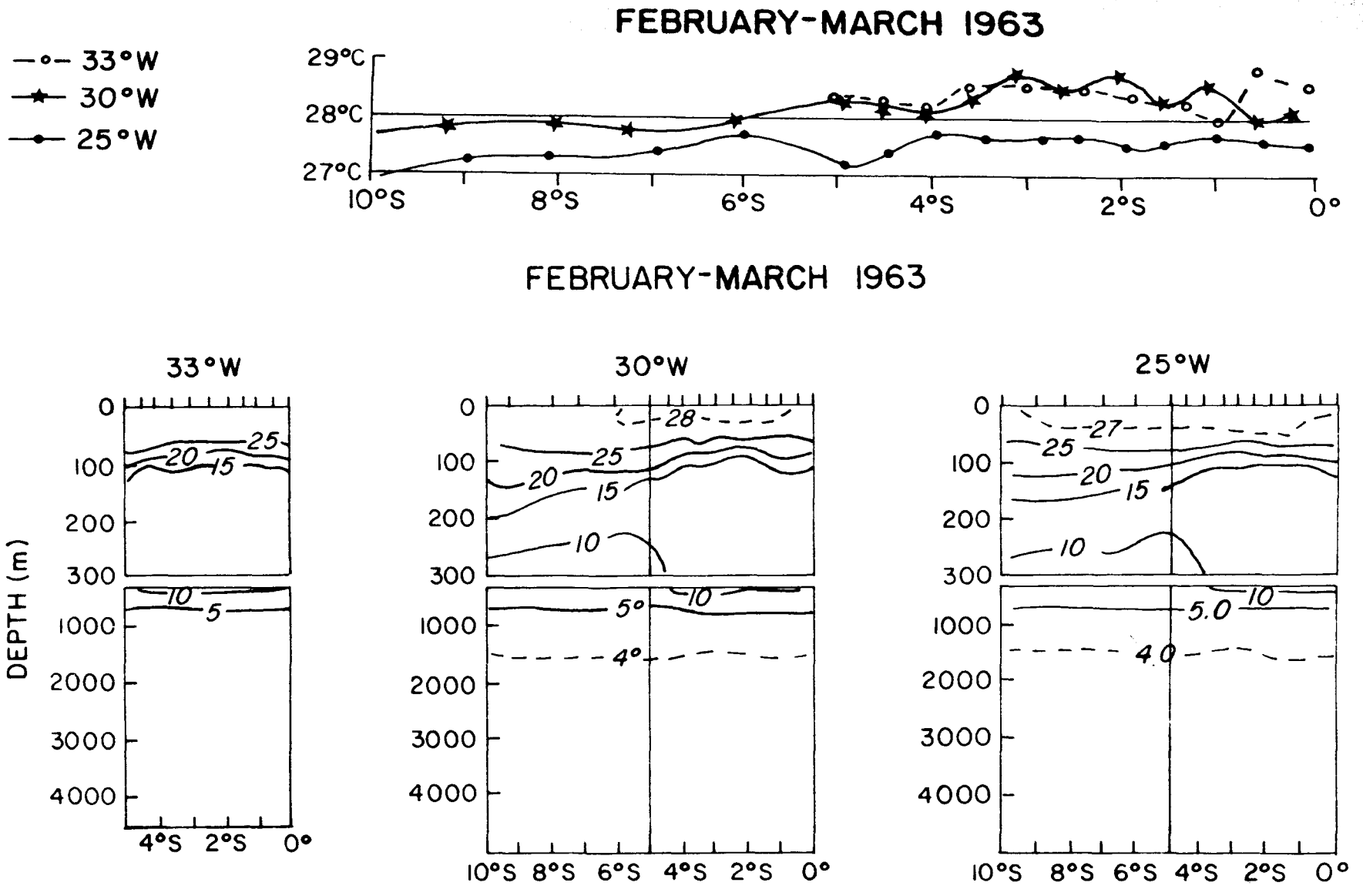

Figure 24: Vertical temperature sections (°C) observed during Equalant I, February - March 1963 and sea-surface temperature traces (Kolesnikov, 1973).

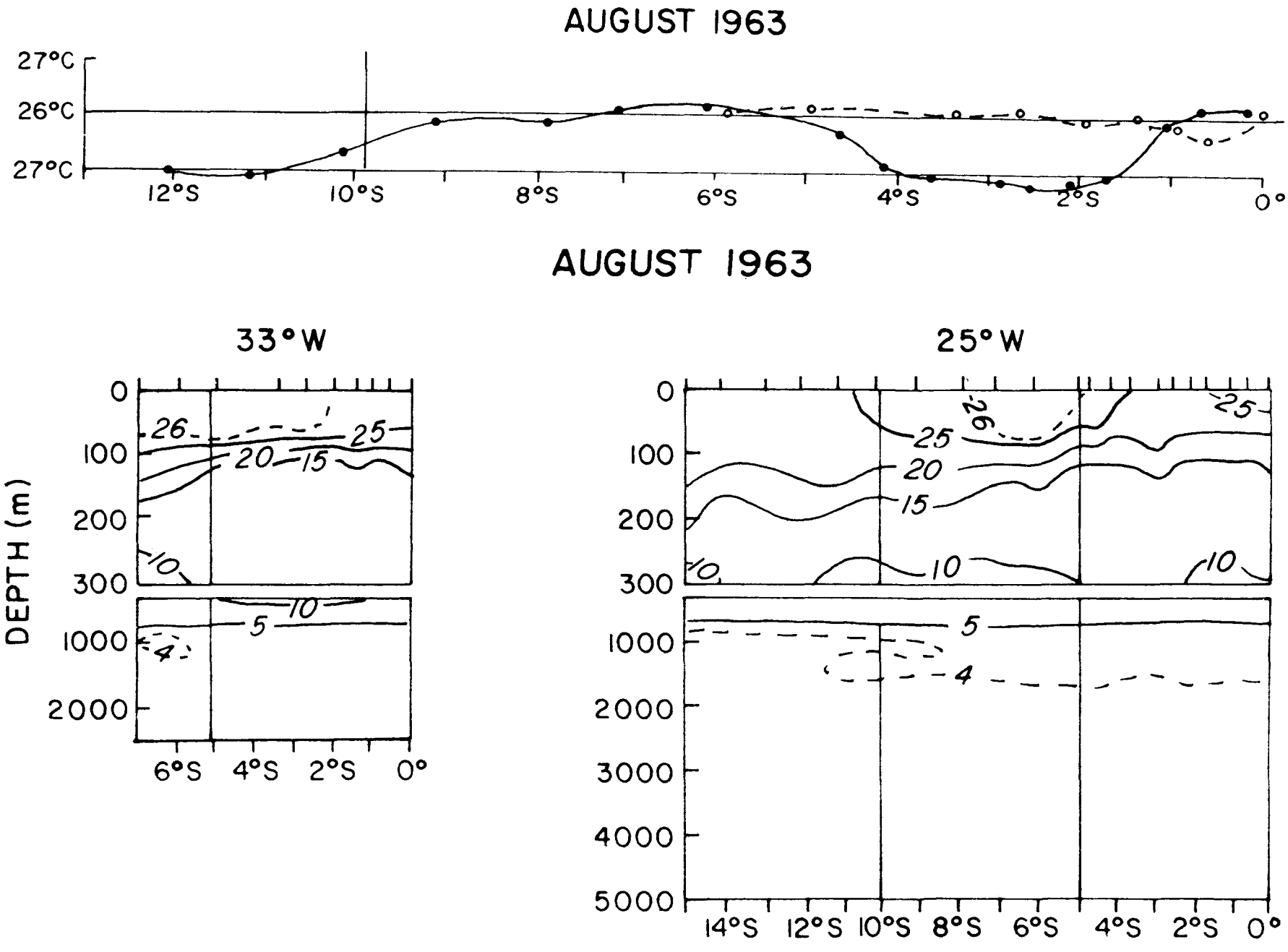

Figure 25: Same as Figure 24, except for Equalant II, August 1963.

8°S

Figure 25: Same as Figure 24, except for Equalant II, August 1963.

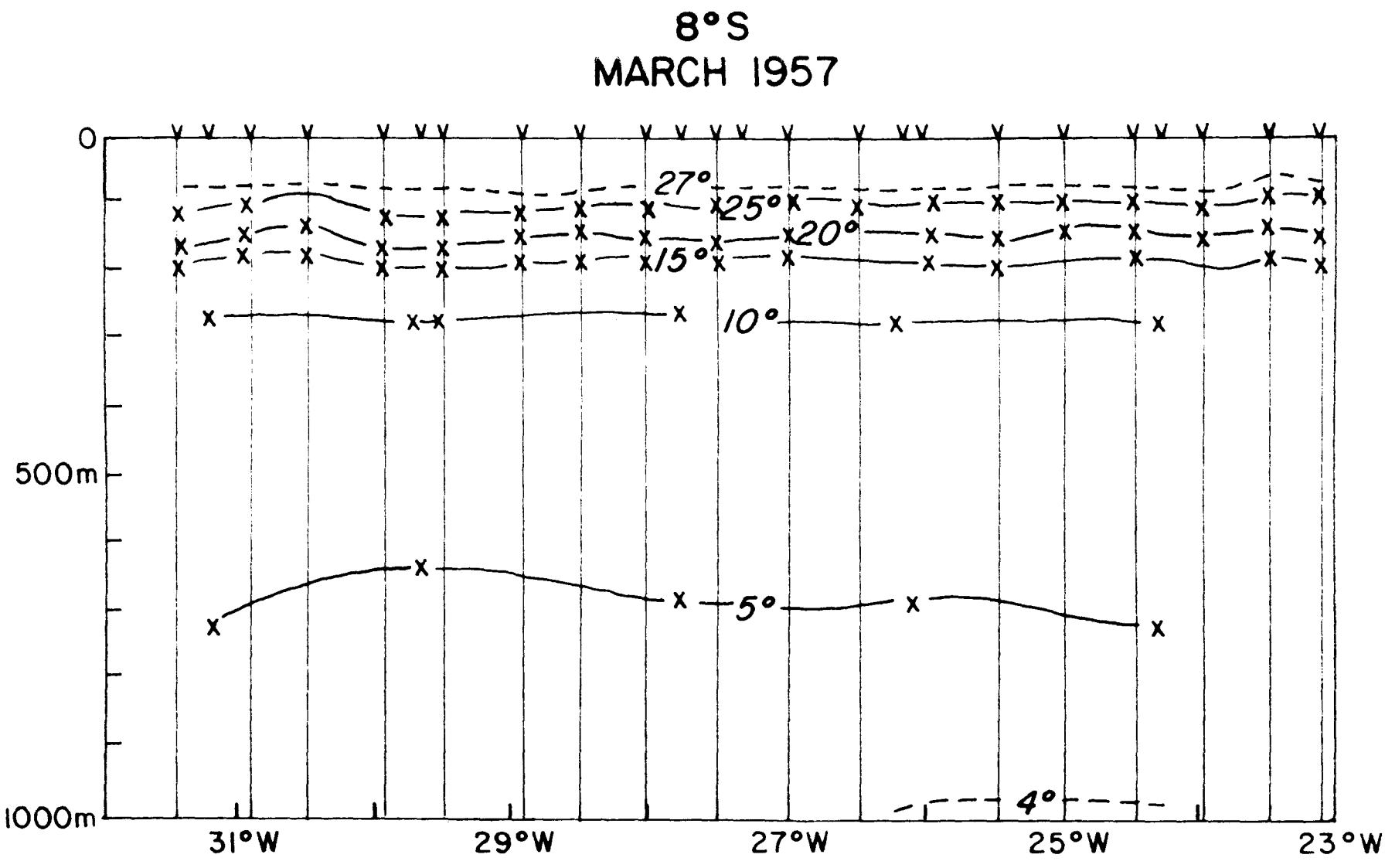

Figure 26: Zonal temperature sections (°C) from March, 1957 (Fuglister, 1960) and September-October, 1971 (Alencastro, 1972).

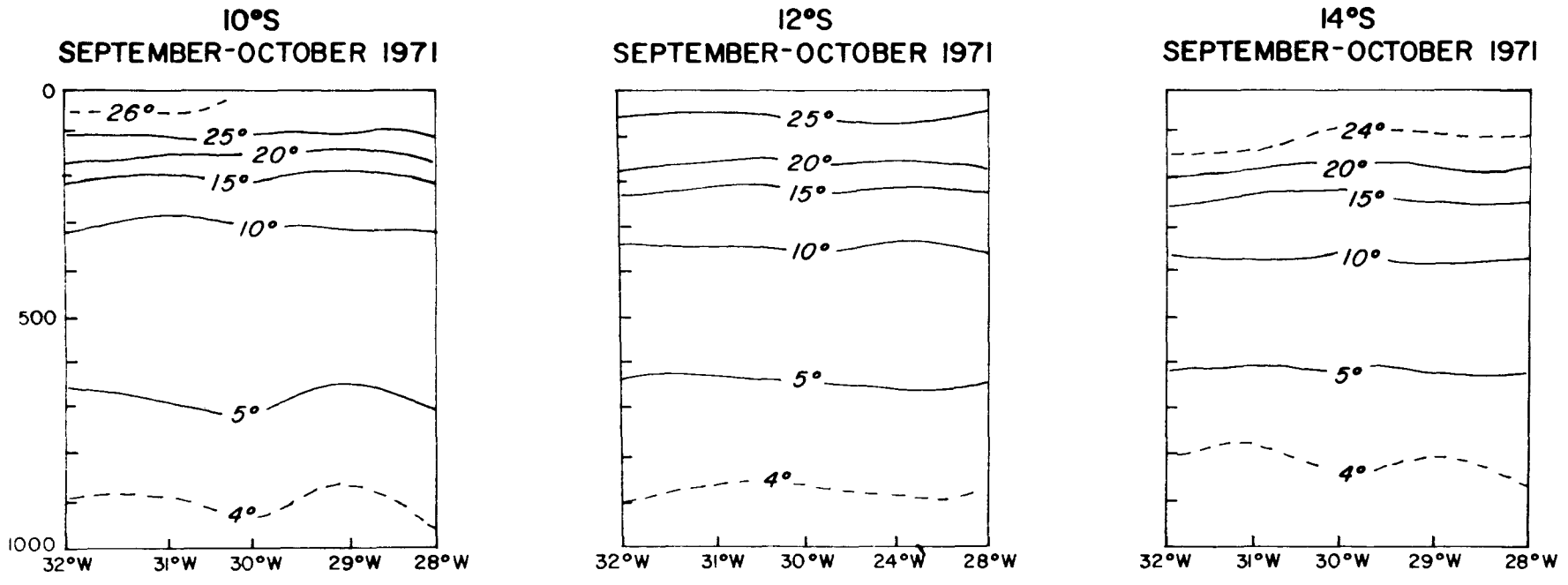

Figure 26: Continued

TABLE: 6 Summary of thermal properties at ATL-1 by subregion (Figure 15). Standard deviations are given for those properties with more than five available data values.

Property	Season	Subregion 11 Latitude 12.5°S	15 11.5°S	19 10.5°S	23 9.5°S	27 8.5°S	31 7.5°S	35 6.5°S	39 5.5°S	43 4.5°S	47 3.5°S
1) Mean SST (°C)	Jan-Mar	27.2	27.6	27.4	27.6	27.2	27.8	27.4	27.5	27.8	27.4
		.7	.4	.2	.5	.2	.5	.2	.6	.4	.5
Standard Deviation	Apr-Jun	26.5	----	24.7	26.5	26.9	26.8	----	----	27.2	27.3
				.4	.2	.3				.4	.2
	Jul-Sep	----	24.4	----	25.5	25.6	25.1	25.6	25.6	26.1	26.0
			.4		.9	1.0			.7	.9	1.2
	Oct-Dec	----	----	----	----	----	----	27.0	27.3	27.5	----
2) T at 900m (°C)	Jan-Mar	4.0	4.0	----	4.1	4.1	4.1	4.1	4.1	4.3	4.2
	Apr-Jun	----	----	4.2	----	4.0	----	----	----	----	----
	Jul-Sep	----	3.9	----	4.1	4.1	----	4.1	----	----	4.3
	Oct-Dec	----	----	4.0	----	----	----	----	----	----	----
3) T at 1000m (°C)	Jan-Mar	4.0	3.8	----	3.9	4.0	4.0	4.0	4.0	----	4.1
	Apr-Jun	----	----	4.0	----	3.9	----	----	----	----	----
	Jul-Sep	----	3.9	----	4.0	3.9	----	4.0	----	----	4.2
	Oct-Dec	----	----	3.8	----	----	----	----	----	----	----
4) Mixed Layer depth (m)	Jan-Mar	37	39	60	52	47	57	46	47	54	48
		19	12	7	8	9	19	11	11	5	10
	Apr-Jun	25	----	----	61	71	80	----	----	71	69
Standard Deviation					12	18				27	16
	Jul-Sep	76	98	95	91	72	70	77	90	96	72
			17	16	14	10				13	24
	Oct-Dec	----	----	90	----	----	----	67	64	71	----
								9	12	14	
5) Thermocline depth (m)	Jan-Mar	108	111	55	107	139	141	115	110	108	92
		53	48	38	38	47	24	14	6	17	11
	Apr-Jun	55	----	----	112	118	90	107	----	95	89
Standard Deviation					35	47				33	7
	Jul-Sep	145	139	149	116	112	115	113	107	123	94
			30	31	21	26		12		16	19
	Oct-Dec	----	----	130	----	----	----	----	126	122	----
									13	11	

In the latitudinal range from 5°S to 10°S the SST ranges from a igh of about 27.5°C in January through March to a low of about 25.5°C in July through September. The 900m temperatures are about 4.1°C in this area, and the 1000m temperatures about 4°C, during all seasons. Thus, the thermal resource to 900m, ranges from about 23.5°C to 21.5°C. The average standard deviation around the resource is about 0.5°C, with a possible maximum in the variability in July-September.

The mixed layer depth in the band 10°S to 5°S ranges from an average of 50m in January-March to an average of 80m in July-September. The variability about these means appears to be of the order 10m. The average thermocline depth over all seasons is of the order 115m with a mean standard deviation of about 25m.

The limited information concerning the current structure in the ATL-1 area is summarized on Table 7, included are possible impacts of the currents on the OTEC operation. The table shows the lack of data relative to all but the grossest characteristics of these currents. The data that do exist, however, suggest these flows could have significant impact on OTEC operations in the area.

VII. Recommendations

The historical data-set is inadequate to generate reliable statistics on the temporal and spatial characteristics of the ATL-1 thermal and current distributions. Therefore, an observational program is required to obtain the data needed in the design effort. As discussed previously, the data collection effort is complicated by the distance to the ATL-1 site and the requirement for data coverage over a larger area than in the case of a moored plant.

The following program is offered as a first iteration in evolving a cost-effective measurement effort. We begin with a discussion of the types of observations to be used, and follow with a detailed description of the first year's observational program. Finally, recommendations for other required studies are given.

SST data derived from satellite would be a cost effective means of obtaining information on the thermal resource if several criteria were established. In particular, the representativeness of SST as a measure of upper layer thermal structure must be demonstrated, because the warm water resource is not merely the surface skin of the ocean. In addition, the ability to distinguish between purely local changes in SST and those caused by advection must be developed. This capability is particularly important if satellite data are to be used in an operational mode, because the current regime will partially determine propulsion requirements.

TABLE 7: Characteristics of Currents in the ATL-1 Area and Their Possible Impact on the OTEC Operation.

Current	Location & Horizontal Structure	Vertical Structure	Temporal Variability	Spatial Variability	Impact
1) South Equatorial Current (SEC)	10°S to 4°N; Africa to Brazil. Gyre has two branches: N-branch crosses the equator & S-branch flows S along S. America. --Broad, slow (50 cms^{-1}) flow to the west.	Maximum velocity at surface apparently decreases monotonically with depth.	From Pilot Charts, maximum in ATL-1 area - May through July; minimum Feb. through April.	GATE data suggest waves exist in SEC near equator, have not been documented in ATL-1 area. Existence of jets, meanders, etc. unknown.	Resource-advection of thermal resource, spatial structure affects recirculation. Design-speeds determine propulsion requirements and current loading on plant. Impact-advection of plant discharges.
2) South Equatorial Counter Current (SECC)	3°S to 7°S (?); coast of Brazil (?) to 10°W (?).	Can occur as a subsurface flow to east with maximum speeds of 60 cms^{-1} at 150 m. Surface flows above can be to west or east.	May be very variable; i.e., at times not observed.	Unknown.	Same as SEC.
3) North Brazilian Current (NBC)	-north coast of Brazil -northern extension of SEC -narrow flow with high speeds (100 cms^{-1}) -may feed Equatorial Undercurrent.	Possibly similar to Gulf Stream.	Unknown.	Unknown.	Impact-advection of plant discharges which originated in SEC.
4) Brazil Current	-east coast of South America -southern extension of SEC -narrow flow with high speeds (100 cms^{-1})	Same as NBC.	Unknown.	Unknown.	Same as NBC.
5) Equatorial Undercurrent (EUC)	-extends across Atlantic, located between 2°N & 2°S -narrow flow, order of 100 km, with high speeds (100 cms^{-1}).	-subsurface speed axis which sometimes surfaces -maximum velocities at about 100 m -surface flows can be to east or west.	-annual signal in phase with wind stress -high frequency (periods 5-10 days) waves observed in GATE.	Axis of EUC meanders about equator.	Impact-advection of plant discharges which have been transported to equator by SEC.

An effort to establish these criteria must necessarily rely on shipboard observations to obtain the data. The ship data also can be complemented by unattended instrumented platforms to increase the spatial and temporal coverage available. Moored surface buoys rigged with thermister chains could provide data on the near-surface thermal structure. Thereby, data on the mixed layer depth and thermocline depth could be obtained as well as data on the thermal resource. If the thermister buoys are placed near one or two current meter moorings, data on the relative importance of advection versus local heating in determining the resource would become available.

Satellite tracked surface drifters also provide a cost-effective method of mapping the surface current distribution. In addition, sea-surface temperature and wind sensors can be mounted on the buoys. The combination of SST and current information available from these buoys can sigificantly increase the spatial coverage needed to address the question of the dominant terms in the heat balance, while providing data on the surface distribution of currents and temperature.

The apparent complicated nature of the subsurface current structure necessitates direct measurements of these flows. Over-the-side current profiling devices provide data on the subsurface temperature structure, and therefore are planned for the cruises to the area. Sampling should be particularly dense in those areas where large shears in the vertical distribution of horizontal currents is expected such as in the SECC. In addition, a longer time-series of current data is to be obtained in the SECC by using a current meter mooring.

Finally, a ship-board observational program to map the large-scale thermal field will provide data on the distribution of mixed layer depth, thermocline depth, and thermal resource. These data are required to evaluate the environmental impact of OTEC operations as well as for input to the design effort. The data are to be obtained by STD and XBT. Furthermore, a ship-of-opportunity program is planned to investigate temporal and spatial variability of the thermal field at shorter time-scales than available from the research vessel cruises. Wyrtki (1978) has shown that data from this type of program also can be used to study current variability if a suitable T-S relation is developed. The STD measurements planned for the larger cruise efforts will supply the needed salinity data.

A preliminary observational program is planned to collect a portion of the impact and design data needed for OTEC. Three cruises aboard the NOAA Ship RESEARCHER through the ATL-1 region are planned for July-August, 1978, February, 1979, and July 1979. The cruises during 1979 will be joint OTEC-FGGE efforts. FGGE is the acronym for the First GARP (Global Atmospheric Research Program) Global Experiment (also called the Global Weather Experiment), a worldwide effort to improve our ability to forecast weather. The tracklines are shown on Figures 27 and 28.

PROPOSED TRACKLINE